Structure and spectroscopic characterization of tetrathia- and tetraselena[8]circulenes as a new class of polyaromatic heterocycles

ARTICLE *in* SPECTROCHIMICA ACTA PART A MOLECULAR AND BIOMOLECULAR SPECTROSCOPY · JUNE 2015

Impact Factor: 2.35 · DOI: 10.1016/j.saa.2015.06.020

Spectrochimica Acta Part A: Molecular and Biomolecular Spectroscopy 151 (2015) 247–261

Contents lists available at ScienceDirect

Spectrochimica Acta Part A: Molecular and Biomolecular Spectroscopy

journal homepage: www.elsevier.com/locate/saa

Structure and spectroscopic characterization of tetrathia- and tetraselena[8]circulenes as a new class of polyaromatic heterocycles

Valentina A. Minaeva [a], Gleb V. Baryshnikov [a,*], Boris F. Minaev [a,e], Nataliya N. Karaush [a], Xiao-Dong Xiong [b], Ming-De Li [d], David Lee Phillips [d], Henry N.C. Wong [b,c]

[a] Department of Organic Chemistry, Bogdan Khmelnitsky National University, blvd. Shevchenko 81, 18031 Cherkasy, Ukraine
[b] Department of Chemistry, State Key Laboratory of Synthetic Chemistry, Center of Novel Functional Molecules, and Institute of Molecular Functional Materials, The Chinese University of Hong Kong, Shatin, New Territories, Hong Kong Special Administrative Region
[c] Shenzhen Municipal Key Laboratory of Chemical Synthesis of Medicinal Organic Molecules & Shenzhen Center of Novel Functional Molecules, Shenzhen Research Institute, The Chinese University of Hong Kong, No. 10, Second Yuexing Road, Shenzhen 518507, China
[d] Department of Chemistry, The University of Hong Kong, Pokfulam Road, Hong Kong Special Administrative Region
[e] Key Laboratory of Engineering Plastics and Beijing National Laboratory for Molecular Science, Institute of Chemistry, Chinese Academy of Sciences, 100190 Beijing, China

HIGHLIGHTS

- Vibrational spectra of tetrathia[8]circulene and tetraselena[8]circulene were measured.
- Vibrational spectra were also calculated and interpreted by the DFT method.
- The comparing with the parent tetraoxa[8]circulene was made.
- Both circulenes possess the bifacial aromatic/antiaromatic nature.
- The first $S_0 \rightarrow S_1$ electronic transition for both molecules is symmetry allowed.

GRAPHICAL ABSTRACT

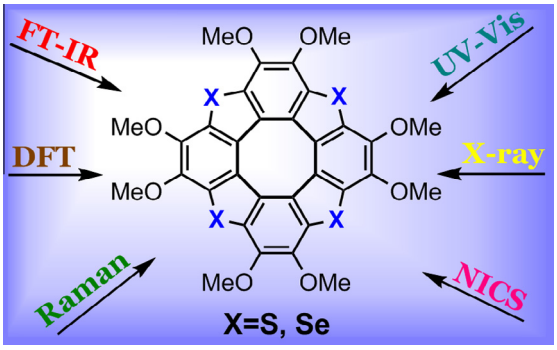

ARTICLE INFO

Article history:
Received 3 December 2014
Received in revised form 3 June 2015
Accepted 9 June 2015
Available online 25 June 2015

Keywords:
Circulene
FT-IR spectra
Raman spectra
UV–vis spectra
DFT calculations
Electronic transition

ABSTRACT

The FTIR, Raman and UV–vis spectra of the recently synthesized tetrathia[8]circulene and tetraselena[8]-circulene compounds have been measured and interpreted in details by the density functional theory (DFT) calculations taking into account the molecular symmetry constrains. The structural and electronic features of the studied compounds have also been discussed in connection with the observed spectroscopic characteristics. Particularly, we have found that despite a slightly non-planar conformation the neutral tetrathia[8]circulene and tetraselena[8]circulene molecules demonstrate bifacial aromatic/antiaromatic nature. The inner octatetraene core is characterized by the presence of paratropic ("antiaromatic") ring currents, whereas the outer macrocycle constructed of benzene, thiophene or selenophene rings possesses the strong magnetically-induced diatropic ("aromatic") ring current. This fact suggests the general electronic and magnetic similarity of the tetrathia- and tetraselena[8]circulenes with the strictly planar isoelectronic tetraoxa[8]circulene and related azaoxa-derivatives discussed earlier. However, the vibrational and UV–vis absorption spectra of the studied circulenes are rather different from those of the parent tetraoxa[8]circulene which indicates a clear manifestation of the symmetry selection rules.

* Corresponding author.
E-mail address: glebchem@rambler.ru (G.V. Baryshnikov).

http://dx.doi.org/10.1016/j.saa.2015.06.020
1386-1425/

1. Introduction

Nowadays the synthesis of new materials for organic electronics is an important and fundamental task of numerous research groups [1–4]. An advantage of implementation of small conjugated compounds is based on possibility of tuning their optical and electric properties by insertion of specific atoms or functional groups or by introduction of side substituents. During last years among the most extensively studied compounds for organic electronics purposes are annelated cyclooctatetraenes which demonstrate the promising properties to be applied in the organic light-emitting diodes (OLEDs) [5] and organic field effect transistors (OFETs) [6–8]. Such cyclooctatetraene derivatives can be classified by two groups: the completely annelated compounds (called also circulenes or heterocirculenes [9] depending on the presence of heteroatoms in their outer perimeter) and partially annelated species (quasicirculenes) [10]. Until nowadays the numerous circulenes (like the Wu's [8]circulene **1** [11], Suzuki's tetrabenzo[8]circulene 2 [12], Nenajdenko's octathia[8]circulene **3** [13] and tetrathiatetraselena[8]circulene **4** [8], Högberg's tetraoxa[8]circulenes **5** and **6** [14,15], Pittelkow's azaoxa[8]circulenes **7** and **8** [16,17] and quasicirculenes (Rajca's thiophene-based quasi[8]circulenes **9**–**11** [18], Iyoda's cyclic tetrathiophene **12** and it's sulfur analogue **13** [19], Torroba's cyclo[n]thiophenes [20], Nishinaga's dithieno[3,4-b:3′,4′-d]thiophene-annelated antiaromatic planar cyclooctatetraene **14** [21], Wilcox's cycloocta[*def*]biphenylene **15** [22], Rabinovitz's cycloocta[*def*]fluorene **16** [23], Wong's heteroatom-bridged tetraphenylenes **17** with different heteroatoms [24] were synthesized and described in details both experimentally and theoretically [22–34]. Moreover, the large number of [8]circulenes have been predicted and thoroughly investigated on the basis of quantum-chemical calculations [10,28,35–42].

A great conjectural application of the circulenes is determined by a possibility of creation of the π-extended one- and two-dimensional materials [12,39,40] which possess quite unusual structural and spectral features and demonstrate the promising semiconducting properties. In this context the synthesis of new members of the circulene family represents the forthcoming task for chemists. One of the possible ways to create new circulenes (as we see from Fig. 1) is a heteroannelation of octamethoxytetraphenylene compound. By this strategy the new tetrathia[8]circulene 18 (**TTC**) and tetraselena[8]circulene 19 (**TSC**) have been synthesized and their key properties have been discussed in the resent publication [43]. However, vibrational and UV–vis spectra of these compounds still are not discussed yet in connection with their structural and electronic peculiarities.

In the present paper we have performed the complete assignment of the IR and Raman spectra of the 18 and 19 species tacking into account their structural and molecular symmetry aspects. Such detailed interpretation of all vibrational modes for the compounds 18 and 19 is an important task for a complete characterization of the ground state properties and for the future analysis of vibronic effects in their absorption and emission spectra which are shortly discussed in the present work. The late aspect being of a large possible potential for their applications in opto-electronics and photonics.

2. Computational details

The structure of the **TTC** and **TSC** molecules together with the basic constituents (benzene, thiophene and selenophene compounds) have been optimized at the B3LYP/6-311++G(d,p) [44–46] level of the density functional theory (DFT) with the control of possible symmetry constrains using the Gaussian09 program package [47]. Vibrational frequencies and the corresponding IR absorption intensities and Raman activities have been calculated for the optimized structures with the same method. All vibrational mode frequencies were found to be real which indicates that a true minimum on hypersurface of the total energy was determined. The calculated vibrational frequencies have been scaled in order to provide a direct comparison with the experimental spectra. The best agreement between the calculated and experimental frequencies can be obtained by using the following scale factors for two separated wave-number regions: 0.95 for the high frequency region (CH stretchings) and 0.98 for the rest of the spectrum (C=C bond stretching in aromatic rings, in-plane and out-of-plane deformations). The scale factors have been calculated as an averaged ratio between the experimentally observed and calculated frequencies of all lines in a particular region of IR and Raman spectra of the studied circulenes. We should note that the calculated values of Raman activities (S_i) are not identical to the experimentally measured Raman intensities of the corresponding vibrational modes. The Raman activities can be easily converted into the relative Raman intensities (I_i) using the following relationship [48]:

$$I_i = \frac{f(v_0 - v_i)^4 S_i}{v_i\left[1 - \exp\left(-\frac{hcv_i}{kT}\right)\right]},$$

where v_0 is the exciting frequency in cm^{-1}, v_i is the vibrational frequency of the *i*-th normal mode, *c*, *h* and *k* are velocity of light, Planck and Boltzmann constants, respectively, *f* is the normalization factor.

The electronic excited state properties of the **TTC** and **TSC** molecules were calculated by the time dependent (TD) DFT method [49] using the same B3LYP hybrid functional and 6-311++G(d,p) basis set. The solvent effect in UV–vis absorption spectra was accounted with the polarizable continuum model (PCM) [50] using dichloromethane as a solvent. Fitting of the electronic absorption spectra curves of the **TTC** and **TSC** molecules was performed using the Gauss-type distribution function and a half-width of 2850 cm^{-1} with the SWizard 4.6 program [51]. The calculated IR and Raman spectra of the studied circulenes have been constructed with the same SWizard 4.6 program [51] using the Lorenz-type distribution function (the band half-width is fixed at 10 cm^{-1}).

The nucleus-independent chemical shift (NICS) indices [52] for the five-, six- and eighth-membered rings of the **TTC** and **TSC** molecules were calculated by the B3LYP/6-311++G(d,p) method with the gauge-independent atomic orbital (GIAO) approximation in order to estimate the local magnetic properties of the studied molecules and to verify the "bifacial" aromaticity of the studied molecules.

3. Results and discussion

3.1. Molecular geometry of the tetrathia[8]circulene and tetraselena[8]circulene molecules

According to the Winberg-Dopper model [9] the shape of the circulenes macrocycle is primarily determined by the sectorial sum (Σ_{sec}) of the cycles which constitute the total macrocycle (the sector of free benzene ring equals 60°, whereas the sector for free thiophene and selenophene molecules equals 45° and 49°, respectively [53,54]. If the sum Σ_{sec} is higher than 360° the circulene becomes non-planar in character manifesting the saddle-shaped structure; but if the sectorial sum Σ_{sec} is lower than 360° the circulene acquires the cone-shaped configuration. When the Σ_{sec} value equals 360° the circulene remains planar structure like the coronene. By this rule the **TTC** and **TSC** molecules possess the sum Σ_{sec} values equal to 420° and 436°, respectively, which should corresponds to a saddle-shaped form of the macrocycle. However the **TTC** is found to be almost planar with a very small

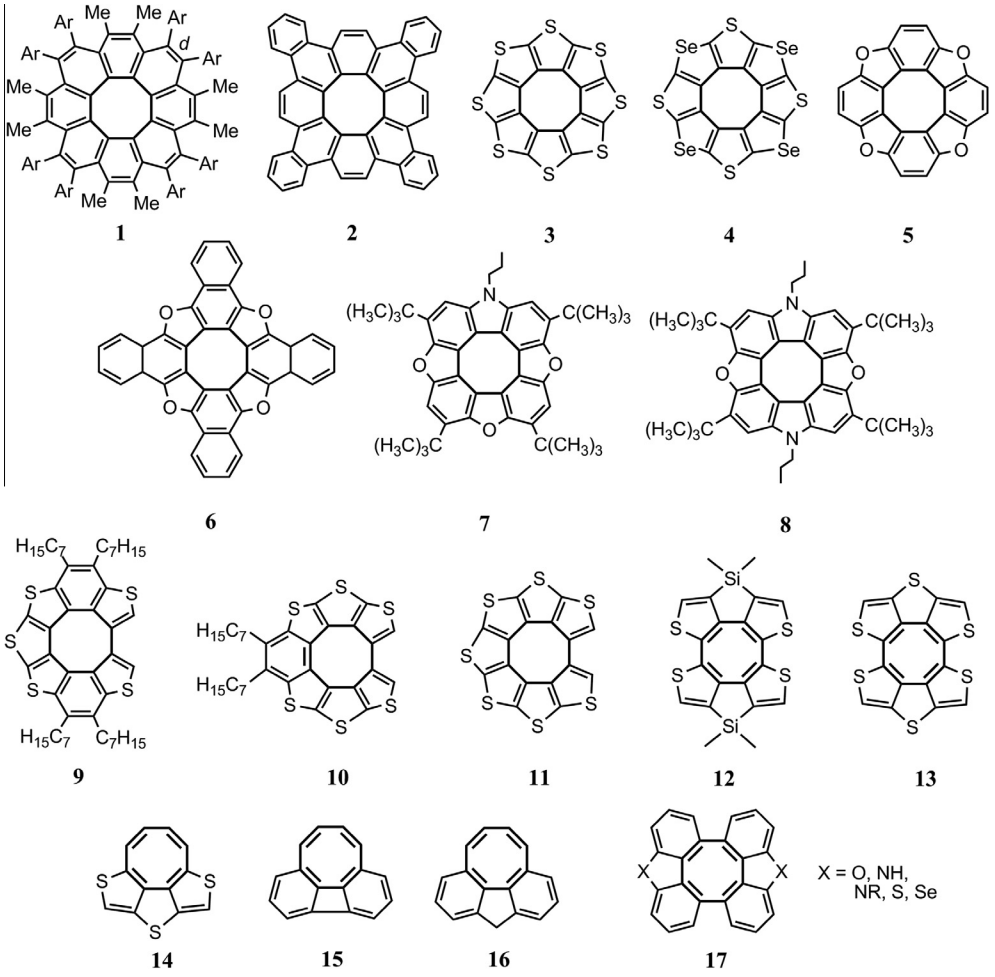

Fig. 1. The structure of various circulenes and quasicirculenes.

deviation from planarity (near the 2°). This small deviation supposed the presence of π-stacking interactions in the crystalline **TTC** observed well by X-ray analysis (Fig. 3a). The same π-stacked dimers are also observed for the **TSC** single crystal with the highly slipping molecules comparing with the **TTC** dimers (Fig. 3b).

The quasi-planar structure of **TTC** macrocycle has been also confirmed by our DFT calculation (Fig. 4) with the negligibly small deviation from planarity (less than 0.5°). This fact can be attributed to the strong decreasing of the benzene ring sector from the 60° to the 44.4° angle in the **TTC** molecule to prevent the strain of macrocycle, whereas the sector for the condensed thiophene ring remains almost unchanged and equals 45.6°. Thus the true Σ_{sec} value for the **TTC** molecule equals to 360° due to a strong

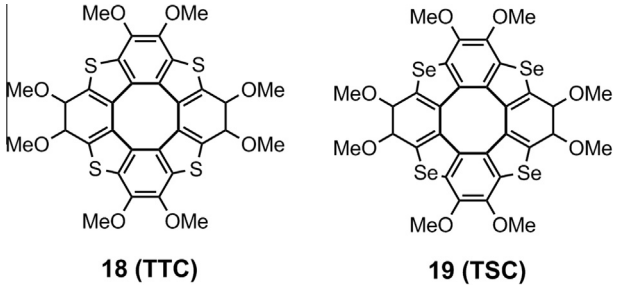

Fig. 2. The structure of new circulenes studied in the present work.

π-conjugation effect. This occasion corresponds to the strong deformation of benzene ring (the condensed CC bonds r_2, r_3 are longer than the outer r_5 and r_6 bonds, Table 1 and Fig. 4).

Because of this we have predicted a significant wave-number and intensity differences between the corresponding frequencies of the free and condensed benzene ring. The same effects have also been observed for the tetraselena[8]circulene (**TSC**) structure and vibrational spectra, but the **TSC** molecule additionally possesses a saddle shaped structure in contrast to the related **TTC** species (the bend angle for the cyclooctatetraene (COT) core of the **TSC** equals 12° according to the X-ray measurements which are in a good agreement with our DFT calculations). In this case the direct comparison of the corresponding vibrational frequencies of the free benzene ring and **TSC** molecule is significantly complicated due to the strong mixing and wave-number shifts of various vibration types.

The five-membered thiophene and selenophene rings demonstrate the trend to extension upon formation of the circulene macrocycle. The r_1 and $r_{3\ (CC)}$ bonds in the **TTC** and **TSC** molecules are increased significantly comparing with the free thiophene and selenophene molecules, whereas the $r_{4\ (CX)}$ bonds remain almost invariable (Table 1). This fact implies the definite specific vibrations of five-membered rings by comparing with the uncondensed thiophene and selenophene molecules.

A special feature of the studied **TTC** and **TSC** molecules is the relatively small alternation of the r_1 and $r_{2\ (CC)}$ bonds in the inner COT core. Indeed, the DFT calculated (r_1–r_2) value for the **TTC**

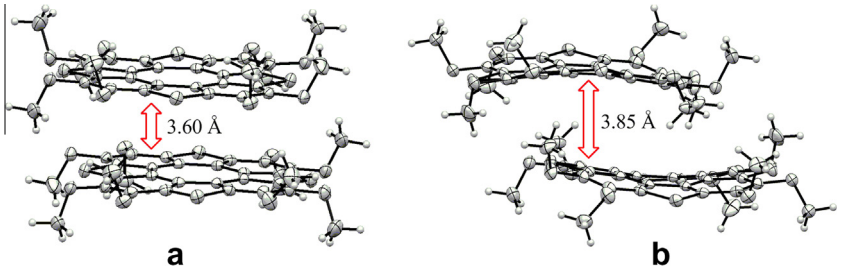

Fig. 3. The π-stacked dimers detected by X-ray analysis in the **TTC** and **TSC** single crystals.

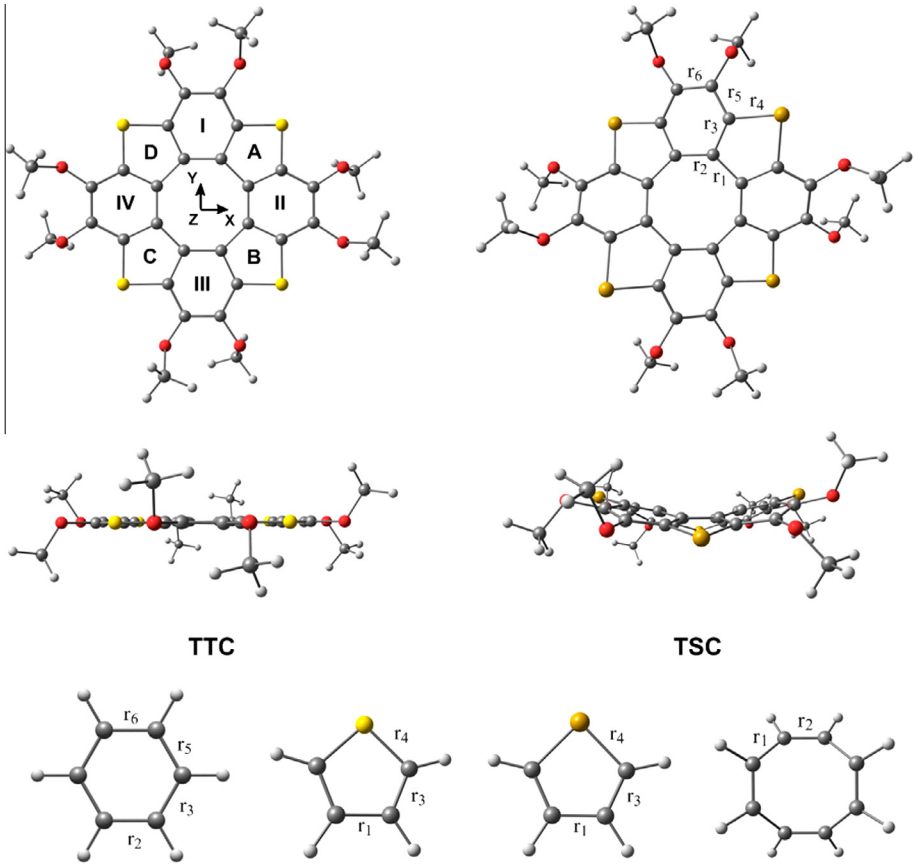

Fig. 4. The B3LYP/6-311++G(d,p) optimized structure of the **TTC** (left side), **TSC** (right side) molecules presented in the top and side projections including the rings and bonds definition and also the choice of axis. The simplest optimized benzene, thiophene, selenophene and cyclooctatetraene structures are presented at the bottom of the figure.

and **TSC** compounds equals 0.038 and 0.041 Å, respectively, which is three times less than for the free cyclooctatetraene molecule (r_1–r_2 = 0.132 Å). Moreover the inner COT core of the studied circulenes demonstrates the slight deviation from planarity relatively to the tub-shaped free COT of the D_{2d} symmetry (Fig. 4). In this way the COT core of the **TTC** and **TSC** molecules possess the weak antiaromatic character comparing with the nonaromatic tub-shaped free COT which is in a good agreement with the NICS indexes calculations [43]. For this reason we have predicted the principal differences between the vibrational spectra of the free D_{2d} COT and its annelated analogue as the part of **TTC** and **TSC** species.

Summing up the structural part of the present paper we have postulated that the vibrational spectra of the **TTC** and **TSC** molecules are highly specific and do not resemble the IR and Raman spectra of the initial free benzene, thiophene and selenophene rings due to the unusual electronic structure of the discussed **TTC** and **TSC** species including the clear π-conjugation effect which induce the strong mixing of the vibrations modes.

3.2. Vibrational spectra of the tetrathia[8]circulene and tetraselena[8]circulene molecules

The substituted **TTC** and **TSC** molecules (Fig. 2) consist of 68 atoms and have 198 normal vibrational modes. According to the D_2 symmetry point group (macrocycle is in the *xy* plane) they can be classified as follows: 51*A*, 49B_1, 49B_2, 49B_3. Vibrations of the B_1, B_2 and B_3 symmetry are active in the IR spectrum. There are no symmetry restrictions for the **TTC** and **TSC** Raman spectra in this symmetry point group. All allowed vibrational modes in IR and Raman spectra of the **TTC** and **TSC** molecules (besides of the low-intensity and low-frequency modes, which are not detectable) are presented and assigned to the observed spectra in Tables

Table 1
Comparison of the B3LYP/6-311++G(d,p) calculated bond lengths (Å) with the experimental data (the second number after slash).

Molecules	$r_{1\ (CC\ long)}$	$r_{2\ (CC\ short)}$	$r_{3\ (CC\ radial)}$	$r_{4\ (CX)}$	$r_{5\ (CC\ side)}$	$r_{6\ (CC\ top)}$
TTC 18[a]	1.479/1.471	1.441/1.434	1.423/1.415	1.735/1.715	1.399/1.398	1.374/1.363
TSC 19[a]	1.487/1.485	1.446/1.445	1.422/1.418	1.879/1.860	1.395/1.395	1.375/1.361
Thiophene[b]	1.427/1.423	–	1.366/1.370	1.733/1.714	–	–
Selenophene[c]	1.432/1.432	–	1.362/1.370	1.876/1.855	–	–
Benzene[d]	–	1.394/1.398	1.394/1.398	–	1.394/1.398	1.394/1.398
$COT_{(D2d)}$[e]	1.472/1.470	1.340/1.337	–	–	–	–

[a] Exp. from Ref. [43] obtained by X-ray analysis.
[b] Exp. from Ref. [53] obtained by microwave spectroscopy.
[c] Exp. from Ref. [54] obtained by microwave spectroscopy.
[d] Exp. from Ref. [55] obtained by gas electron diffraction.
[e] Exp. from Ref. [56] obtained by femtosecond rotational coherence spectroscopy.

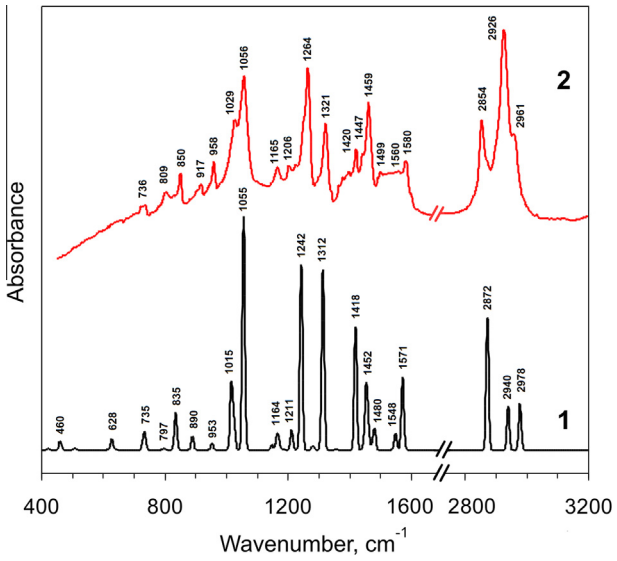

Fig. 5. Calculated (curve **1**, black line) and experimental (curve **2**, red line) IR spectra of the **TTC** compound. (For interpretation of the references to color in this figure legend, the reader is referred to the web version of this article.)

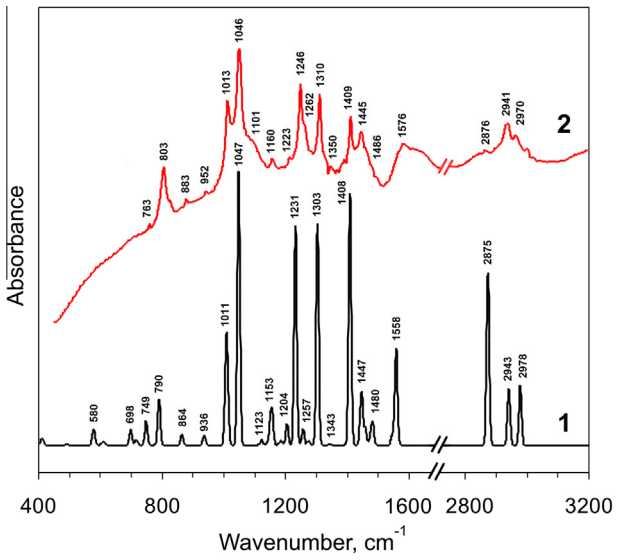

Fig. 6. Calculated (curve **1**, black line) and experimental (curve **2**, red line) IR spectra of the **TSC** compound. (For interpretation of the references to color in this figure legend, the reader is referred to the web version of this article.)

2 and 3, respectively. The full tables for all modes are given in Supplementary materials.

Since the **TTC** molecule is almost planar (its effective symmetry group is practically close to the D_{2d} point group) the B_3 and B_2 modes are practically degenerate. In **TSC** they are slightly split because of more prominent deviation from molecular planarity.

The calculated IR spectra for the **TTC** and **TSC** molecules are presented in Figs. 5 and 6, respectively (curve 1) for the spectral region 3200–400 cm^{-1} and they are compared with the experimental IR spectra (curve 2) of these species. The calculated and experimental Raman spectra for the **TTC** and **TSC** molecules are presented in Figs. 7 and 8, respectively. In the range 1200–800 cm^{-1} of the Raman spectra there are many weak features at the level of noise; nevertheless we have identified them as a set of clear signals which have the corresponding low intensity in DFT calculated spectra. In Figs. 7 and 8 the resonance Raman spectra of samples include the asterisk (*) marks which indicate a subtraction of artifact signals from the solvent and the excited laser line. Accordingly, the genuine Raman bands (they are clearly identified in the calculated spectra) are overlapped by the seeming asterisk-marked signals which complicate the band assignment in the region 1410–1450 cm^{-1}.

3.2.1. Vibrations of the Ar–O–CH_3 substituents

For the methoxyaryl-groups Ar–O–CH_3 the following types of vibrations are observed: stretching and bending C–H vibrations, rocking and torsional vibrations of the CH_3 groups, and C–O skeletal vibrations. Because of large amount of such substituent groups and triple times larger number of C–H bonds, we have many degenerate vibrations of these types.

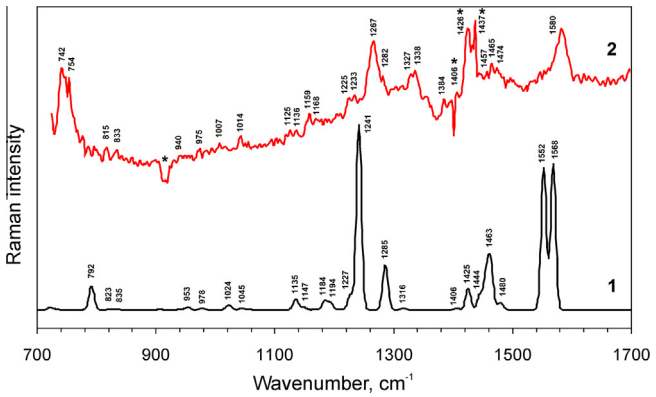

Fig. 7. Calculated (curve **1**, black line) and experimental (curve **2**, red line) Raman spectra of the **TTC** compound. The asterisk (*) marks subtraction artifacts or laser line. (For interpretation of the references to color in this figure legend, the reader is referred to the web version of this article.)

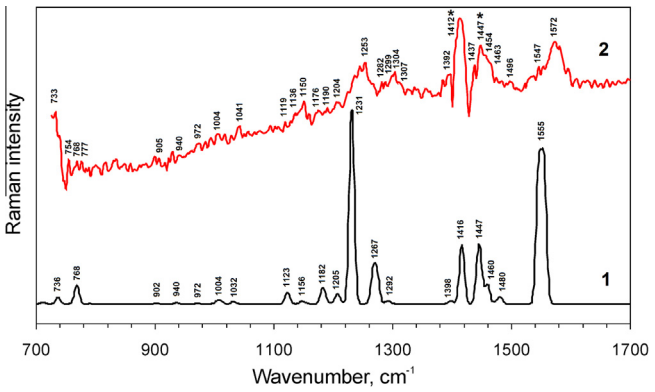

Fig. 8. Calculated (curve **1**, black line) and experimental (curve **2**, red line) Raman spectra of the **TSC** compound. The asterisk (*) marks subtraction artifacts or laser line. (For interpretation of the references to color in this figure legend, the reader is referred to the web version of this article.)

3.2.1.1. The CH_3 vibrations. These vibrations for the Ar–O–CH_3 groups can be usually found in the range 3005–2815 cm^{-1} (CH stretching), 1485–1420 cm^{-1} (CH deformation (or CH bending) vibrations), 1235–855 cm^{-1} (rocking vibrations) and below 265 cm^{-1} (torsional vibrations) [57]. In spite of huge degeneracy and a small number of the corresponding observed IR bands an analysis of such manifolds is still interesting for structural chemistry. This illustrates the profound depth of molecular vibrations theory and the power of modern DFT techniques.

The CH_3 asymmetric stretching vibrations in the **TTC** molecule according to our DFT calculation have to be observed in the region 2978–2939 cm^{-1} (Table 2, ν_{198}–ν_{183}) being comparable with the general analysis of Ref. [57] In the calculated IR spectrum of **TTC** (Fig. 5, curve 1) the asymmetric CH_3 stretching vibrations provide only two well-resolved bands of middle intensity with a maximum at 2978 and 2940 cm^{-1}. In experimental IR spectrum of the **TTC** molecule (Fig. 5, curve 2) the asymmetric CH_3 stretching vibrations are observed as a single wide band of strong intensity with a maximum at 2926 cm^{-1} and a shoulder from the right side at 2961 cm^{-1} indicating a reasonable good agreement with DFT prediction. The symmetric CH_3 stretching vibrations in the calculated IR spectrum of **TTC** (Table 2, ν_{182}–ν_{175}) are indicated in the narrow region 2873–2872 cm^{-1} (exp.: 2854 cm^{-1}) producing the band of medium intensity. The complicated structure of this IR absorption is clearly seen in the experimental band shape (Fig. 5, curve 2), where some frequencies are slightly shiffed by 14–19 cm^{-1} in respect to DFT prediction (Table 2).

In contrast, the corresponding IR bands in the observed **TSC** spectrum are in a good agreement with the calculated DFT data (Table 3). According to our calculation, the asymmetric and symmetric CH_3 stretching vibrations of **TSC** molecule have to appear in the IR spectrum at the frequencies close to those of **TTC** (Tables 2 and 3). However, in the experimental IR spectrum of **TTC** the corresponding vibration bands are shifted to the lower frequency (by 22–9 cm^{-1}, respectively) in comparison with the IR spectra of **TSC** where the calculated values of the band maxima of the CH_3 stretching vibrations are close to experimental splitting. Such shifts may be explained by stronger intermolecular interactions in the **TTC** crystal. Because of non-planar structure of **TSC** molecule (Fig. 3) the intermolecular distance in the crystal is longer than in the **TTC** species and π-stacking interactions in **TSC** crystal are weaker. The CH_3 stretching vibrations in **TTC** crystal are more perturbed by intermolecular forces; particulary the presence of $CH_3\cdots C$ intermolecular interactions (Fig. 3) provides deviations from the calculated spectra of free **TTC** molecule.

As follows from Fig. 6 the CH_3 stretching vibrations of **TSC** provide less intense experimental IR absorption bands in comparison with **TTC**, which is partially explained by lower calculated intensity for the first IR band (Tables 2 and 3, ν_{197}, ν_{196}). More tight $CH_3\cdots C$ intermolecular interactions in **TTC** crystal provide additional CH_3 bond polarization and enhancement of IR intensity for the corresponding modes. Moreover, in the crystal the splitting of many close lying bands occurs which are practically degenerate in free molecules (Tables 2 and 3); this provides an additional broadening of the bands.

The asymmetric CH_3 deformation vibrations, $\delta(CH_3)$ are calculated in the IR spectrum of the **TTC** molecule as 17 transitions in the range 1480–1458 cm^{-1} (Table 2, ν_{166}–ν_{150}). Many of them are weak or forbidden. Thus, they give rise in the calculated IR spectrum just only to two weak vibration bands at 1480 cm^{-1} (exp.: 1499 cm^{-1}) and 1458 cm^{-1}. The late band is overlapped by the absorption feature of strong intensity occurring at 1452 cm^{-1} (exp.: 1459 cm^{-1}), which belong to symmetric $\delta(CH_3)$ mode, mixed with the asymmetric ν(C=C) vibration in benzene rings (Table 2, ν_{149}, ν_{148}, Fig. 5). In the calculated and experimental IR spectra **TSC** (Fig. 6) this band (calc.: 1447 and 1446 cm^{-1}, exp.: 1445 cm^{-1}) demonstrates a weak low-frequency shift (Table 3, ν_{150}, ν_{148}) and the lower absorption intensity.

In the range 1425–1406 cm^{-1} (Table 2, ν_{142}–ν_{139}) the symmetric CH_3 deformations are also mixed with the asymmetric ν(C=C) vibrations in benzene rings. The corresponding band appears in the experimental infrared spectrum of **TTC** at 1420 cm^{-1} with the medium intensity (Fig. 5, curve 2); however in the calculated IR spectrum (calc.: 1418 cm^{-1}) its intensity is definitely overestimated (Fig. 5, curve 1). The corresponding band in the IR spectra of **TSC** (Fig. 6, calc.: 1408 cm^{-1}, exp.: 1409 cm^{-1}) is shifted by 10 cm^{-1} to the low-frequency range in comparison with **TTC** and also show the higher calculated intensity (Table 3, ν_{141}, ν_{140}). The reason for the shift is determined by a large length difference of the benzene ring C=C bonds (Table 1, r_2) conjugated with the [8]circulene moiety, which support our assignment of the mixed nature of the $\delta(CH_3)$ modes. As far as IR intensity concerns the discrepancies between theory and experiment are often observed for CH vibrations [30–34].

Asymmetric CH_3 deformation in the Raman spectrum of the **TTC** molecule is determined by the normal modes ν_{158} and ν_{150} of the *A* symmetry with the frequencies 1463 and 1455 cm^{-1}, respectively (Table 2). The corresponding resulting band of medium intensity (Fig. 7) occurs as a wide feature at 1463 cm^{-1} in DFT simulation (exp.: 1465 and 1457 cm^{-1}). A very weak shoulder to the right (ν_{166}, ν_{165}, calc.: 1480 cm^{-1}) also belongs to asymmetric CH_3 deformations (exp.: 1474 cm^{-1}).

The normal modes ν_{166}–ν_{151} in the **TSC** molecule in the range 1482–1458 cm^{-1} (Table 3) are responsible for the asymmetric deformations of methyl groups; in the simulated Raman spectrum (Fig. 8) they also provide a weak band 1480 cm^{-1} (exp.: 1496, 1482, 1479 and 1474 cm^{-1}) and a shoulder 1460 cm^{-1} (exp.: 1463 cm^{-1}) at the symmetric deformation band 1447 cm^{-1} of medium intensity, containing a contribution of the C=C asymmetric stretching vibrations in benzene rings. We can see that detailed comparison between theory and experiment provides many interesting details which are usually considered as a noise in Raman and IR spectra.

The CH_3 symmetric deformation modes ν_{142} and ν_{139}, being mixed with the stretching vibrations of the C=C bonds of benzene and thiophene rings (Table 2), gives a well-seeing band 1425 cm^{-1} (exp.: 1426 cm^{-1}) and very weak band 1406 cm^{-1} (exp.: 1406 cm^{-1}) in the Raman spectrum of **TTC** molecule (Fig. 7). Accordingly, in the Raman spectrum of **TSC** molecule (Fig. 8) we assign a more intense line 1416 cm^{-1} (exp.: 1412 cm^{-1}) and weak line 1398 cm^{-1} (exp.: 1392 cm^{-1}). Very important to stress that the

Table 2
Calculated and experimental vibrational modes of tetrathia[8]circulene.

Nu.	Sym.	Fre.	I_{IR}	S_i	I_i	Exp.	Assignment
ν_{198}	A	2978	0	630.6	$9.9 \cdot 10^{-2}$		CH_3 str., as., I–IV
ν_{197}	B_3	2978	75.5	0.03	$4.9 \cdot 10^{-6}$	2961 IR	CH_3 str., as., II, IV
ν_{196}	B_2	2978	75.7	0.03	$4.9 \cdot 10^{-6}$	2961 IR	CH_3 str., as., I, III
ν_{189}	B_3	2940	61.1	35.8	$5.7 \cdot 10^{-3}$	2926 IR	CH_3 str., as., II, IV
ν_{188}	B_2	2940	61.1	35.9	$5.7 \cdot 10^{-3}$	2926 IR	CH_3 str., as., I, III
ν_{185}	B_2	2939	20.5	13.9	$2.2 \cdot 10^{-3}$	2926 IR	CH_3 str., as., II, IV
ν_{184}	B_3	2939	20.5	13.9	$2.2 \cdot 10^{-3}$	2926 IR	CH_3 str., as., I, III
ν_{182}	A	2873	0	1259.3	$2.1 \cdot 10^{-1}$		CH_3 str., s., I–IV iph.
ν_{181}	B_2	2873	125.1	17.1	$2.8 \cdot 10^{-3}$	2854 IR	CH_3 str., s., I, III oph.
ν_{180}	B_3	2873	125.1	17.1	$2.8 \cdot 10^{-3}$	2854 IR	CH_3 str., s., II, IV oph.
ν_{178}	B_1	2872	237.2	0.0005	$8.2 \cdot 10^{-8}$	2854 IR	CH_3 str., s., I oph. and III oph., II oph. and IV oph.
ν_{175}	B_1	2872	0.007	16.4	$2.7 \cdot 10^{-3}$		CH_3 str., s., I oph. and III oph., II oph. and IV oph.
ν_{173}	B_2	1571	143.7	3.5	$1.3 \cdot 10^{-3}$	1580 IR	CC str., s., I, III oph.
ν_{172}	B_3	1571	143.7	3.5	$1.3 \cdot 10^{-3}$	1580 IR	CC str., s., II, IV oph.
ν_{171}	A	1568	0	1650.9	$5.9 \cdot 10^{-1}$	1580 R	CC str., s., I–IV iph.
ν_{170}	B_1	1552	0	1605.9	$5.9 \cdot 10^{-1}$	1580 R	CC str., s., I–IV, $C^{\alpha}C^{\beta}$ and $C^{\alpha'}C^{\beta'}$ str., s., CSC bend., A, C iph. and B, D, iph.
ν_{169}	B_2	1548	29.3	9.7	$3.6 \cdot 10^{-3}$	1560 IR	CC str., s., II, IV iph.
ν_{168}	B_3	1548	29.3	9.7	$3.6 \cdot 10^{-3}$		CC str., s., I, III iph.
ν_{167}	B_1	1546	10.4	0.0004	$1.5 \cdot 10^{-7}$		CC str., s., I, III oph., II, IV oph., $C^{\alpha}C^{\beta}$ and $C^{\alpha'}C^{\beta'}$ str., as., A, B, C, D
ν_{166}	A	1480	0	33.4	$1.3 \cdot 10^{-2}$	1474 R	CH_3 bend, as., I–IV
ν_{165}	A	1480	0	29.8	$1.2 \cdot 10^{-2}$	1474 R	CH_3 bend, as., I–IV
ν_{164}	B_2	1480	38.8	2.8	$1.1 \cdot 10^{-3}$	1499 IR	CH_3 bend, as., I, III
ν_{163}	B_3	1480	38.8	2.8	$1.1 \cdot 10^{-3}$	1499 IR	CH_3 bend, as., II, IV
ν_{158}	A	1463	0	494.4	$2.0 \cdot 10^{-1}$	1465 R	CH_3 bend, as., I–IV
ν_{157}	B_3	1461	22.5	9.0	$3.6 \cdot 10^{-3}$	1459 IR	CH_3 bend, as., II, IV
ν_{156}	B_2	1461	22.5	9.0	$3.6 \cdot 10^{-3}$	1459 IR	CH_3 bend, as., I, III
ν_{154}	B_1	1458	0.001	47.6	$1.9 \cdot 10^{-2}$	1457 R	CH_3 bend, as., I–IV
ν_{153}	B_2	1458	25.7	1.6	$6.4 \cdot 10^{-4}$	1459 IR	CH_3 bend, as., II, IV
ν_{152}	B_3	1458	25.7	1.6	$6.4 \cdot 10^{-4}$	1459 IR	CH_3 bend, as., I, III
ν_{150}	A	1455	0	318.8	$1.3 \cdot 10^{-1}$	1457 R	CH_3 bend, as., I–IV
ν_{149}	B_3	1452	118.2	0.4	$1.4 \cdot 10^{-4}$	1459 IR	CH_3 bend, s., II, IV oph., I oph., III oph., CC str., as., II, IV, oph.
ν_{148}	B_2	1452	118.2	0.4	$1.4 \cdot 10^{-4}$	1459 IR	CH_3 bend, s., I, III oph., II oph., IV oph., CC str., as., I, III, oph.
ν_{147}	A	1448	0	33.2	$1.3 \cdot 10^{-2}$	1437 R	CH_3 bend, s., I, III iph., II, IV iph.
ν_{145}	B_1	1444	0	135.7	$5.4 \cdot 10^{-2}$	1437 R	CH_3 bend, s., I oph., III oph., II oph., IV oph.
ν_{144}	B_3	1443	2.3	2.3	$9.3 \cdot 10^{-4}$	1447 IR	CH_3 bend, s., I oph., III oph.
ν_{143}	B_2	1443	2.3	2.3	$9.3 \cdot 10^{-4}$	1447 IR	CH_3 bend, s., II oph., IV oph.
ν_{142}	A	1425	0	236.4	$9.6 \cdot 10^{-2}$	1426 R	CH_3 bend, s., I–IV iph., CC str., as., I–IV iph., $C^{\alpha}C^{\beta}$, $C^{\alpha'}C^{\beta'}$ str., iph. and $C^{\beta}C^{\beta'}$ str. oph., CSC bend iph.
ν_{141}	B_2	1418	243.6	0.4	$1.5 \cdot 10^{-4}$	1420 IR	CH_3 bend, s., I, III oph., CC str., as., I, III
ν_{140}	B_3	1418	243.6	0.4	$1.5 \cdot 10^{-4}$	1420 IR	CH_3 bend, s., II, IV oph., CC str., as., II, IV
ν_{139}	A	1406	0	15.8	$6.5 \cdot 10^{-3}$	1406 R	CH_3 bend, s., I, III and II, IV oph., CC str., as., I, III and II, IV oph.
ν_{137}	A	1316	0	18.8	$8.4 \cdot 10^{-3}$	1338 R	CC str., as., Kekule, I–IV, iph.
ν_{136}	B_3	1312	357.4	0.6	$2.7 \cdot 10^{-4}$	1321 IR	CC str., as., Kekule, II, IV oph.
ν_{135}	B_2	1312	357.4	0.6	$2.7 \cdot 10^{-4}$	1321 IR	CC str., as., Kekule, I, III oph.
ν_{134}	B_1	1288	0	240.3	$1.1 \cdot 10^{-1}$	1327 R	$C^{\beta}C^{\beta'}$ srt., A, C and B, D, oph.
ν_{133}	A	1285	0	291.9	$1.3 \cdot 10^{-1}$	1282 R	CC str., as., Kekule, I, III and II, IV, oph., $C^{\alpha}C^{\beta}$ and $C^{\alpha'}C^{\beta'}$ str., as., A, B, C, D
ν_{132}	B_3	1280	7.8	1.5	$6.9 \cdot 10^{-4}$		CC str., as., I, III, $C^{\beta}C^{\beta'}$ str., II, IV oph.
ν_{131}	B_2	1280	7.8	1.5	$6.9 \cdot 10^{-4}$		CC str., as., II, IV, $C^{\beta}C^{\beta'}$ str., I, III oph.
ν_{130}	B_2	1242	366.0	0.08	$3.9 \cdot 10^{-5}$	1264 IR	CC str., as., I, III oph., CH_3 rock., I–IV
ν_{129}	B_3	1242	366.0	0.08	$3.9 \cdot 10^{-5}$	1264 IR	CC str., as., II, IV oph., CH_3 rock., I–IV
ν_{128}	A	1241	0	2099.0	1.0	1267 R	$C^{\alpha}C^{\beta}$, $C^{\alpha'}C^{\beta'}$ str., iph. and $C^{\beta}C^{\beta'}$ str., oph., ct. def., s., CS str., s., iph., CH_3 rock., I–IV
ν_{127}	B_1	1227	0	168.9	$8.2 \cdot 10^{-2}$	1233 R	$C^{\alpha}C^{\beta}$, $C^{\alpha'}C^{\beta'}$ str., s., CS str., s., I, III and II, IV, oph., ct. def., as., CH_3 rock., I–IV
ν_{126}	B_2	1211	9.8	5.0	$2.4 \cdot 10^{-3}$	1206 R	I, III benz. def. s., oph., CH_3 rock., II, IV, $C^{\alpha}C^{\beta}$, $C^{\alpha'}C^{\beta'}$ str., iph. and $C^{\beta}C^{\beta'}$ str. oph., CS str., s.
ν_{125}	B_3	1211	9.8	5.0	$2.4 \cdot 10^{-3}$	1206 R	II, IV benz. def. s., oph., CH_3 rock., I, III, $C^{\alpha}C^{\beta}$, $C^{\alpha'}C^{\beta'}$ str., iph. and $C^{\beta}C^{\beta'}$ str. oph., CS str., s.
ν_{124}	B_1	1211	57.5	0	0	1206 IR	CH_3 rock., I–IV
ν_{123}	B_1	1194	0	69.8	$3.5 \cdot 10^{-2}$	1168 R	CH_3 rock., I–IV
ν_{119}	A	1184	0	102.4	$5.2 \cdot 10^{-2}$	1159 R	CH_3 rock., I–IV
ν_{115}	B_1	1164	55.2	0	0	1165 IR	CH_3 rock., I–IV, CS str., as.
ν_{110}	A	1147	0	17.1	$8.9 \cdot 10^{-3}$	1136 R	CH_3 rock., I–IV
ν_{109}	B_2	1147	11.2	2.4	$1.2 \cdot 10^{-3}$		CH_3 rock., I, III
ν_{108}	B_3	1147	11.2	2.4	$1.2 \cdot 10^{-3}$		CH_3 rock., II, IV
ν_{107}	A	1147	0	7.8	$4.1 \cdot 10^{-3}$	1136 R	CH_3 rock., I–IV
ν_{106}	B_1	1135	0	121.5	$6.4 \cdot 10^{-2}$	1125 R	C_{benz}–O str., I oph., II oph., III oph., IV oph., I–IV benz. def., as., $C^{\beta}C^{\beta'}$ str., A, C and B, D, oph., CH_3 rock., I–IV
ν_{105}	B_2	1055	459.8	2.1	$1.2 \cdot 10^{-3}$	1056 IR	H_3C–O str., I iph., III iph., II oph., IV oph., ct. sw.
ν_{104}	B_3	1055	459.8	2.1	$1.2 \cdot 10^{-3}$	1056 IR	H_3C–O str., I oph., III oph., II iph., IV iph., ct. sw.
ν_{103}	A	1045	0	16.9	$9.8 \cdot 10^{-3}$	1041 R	H_3C–O str., I–IV iph., I–IV benz. def., s., iph., CS str., s., iph.
ν_{102}	B_2	1024	55.2	14.5	$8.6 \cdot 10^{-3}$	1029 IR 1012 R	H_3C–O str., I iph., III iph., II oph., IV oph., I, III benz. def., s., oph., ct., II, IV benz. def. as., CS str., s.
ν_{101}	B_3	1024	55.2	14.5	$8.6 \cdot 10^{-3}$	1029 IR 1012 R	H_3C–O str., I oph., III oph., II iph., IV iph., II, IV benz. def., s., oph., ct., I, III benz. def. as., CS str., s.
ν_{100}	A	1022	0	29.6	$1.8 \cdot 10^{-2}$	1007 R	H_3C–O str., I, III iph., II, IV iph., I, III and II, IV benz. def., s., oph., CS str., as.
ν_{99}	B_1	1015	259.6	0	0	1029 IR	H_3C–O str., I oph., II oph., III oph., IV oph., I–IV benz. def., as., CS str., as.
ν_{98}	B_1	978	0	19.0	$1.2 \cdot 10^{-2}$	975 R	H_3C–O str., I oph., II oph., III oph., IV oph., I–IV benz. def., as., CSC bend., A, C and B, D oph.
ν_{97}	B_3	953	13.2	14.9	$9.6 \cdot 10^{-3}$	958 IR 940 R	H_3C–O str., I oph., III oph., I, III benz. def. as., II, IV benz. def., s., oph., CH_3 rock., I, III

(*continued on next page*)

Table 2 (*continued*)

Nu.	Sym.	Fre.	I_{IR}	S_i	I_i	Exp.	Assignment
ν_{96}	B_2	953	13.2	15.0	$9.7 \cdot 10^{-3}$	958 IR 940 R	H_3C–O str., II oph., IV oph., II, IV benz. def., as., I, III benz. def. s., oph., CH_3 rock., II, IV
ν_{91}	B_1	890	55.0	0	0	917 IR	H_3C–O str., I oph., II oph., III oph., IV oph., I–IV benz., ct. def., as., CH_3 rock., I–IV, CS str., as.
ν_{90}	B_3	835	74.0	3.2	$2.4 \cdot 10^{-3}$	850 IR 833 R	CS str., as., I–IV, displacement of I, III benz. moieties along y-direction, ct. def. as., CH_3 rock., I, III
ν_{89}	B_2	835	74.0	3.2	$2.4 \cdot 10^{-3}$	850 IR 833 R	CS str., as., I–IV, displacement of II, IV benz. moieties along y-direction, ct. def. as.
ν_{88}	B_1	823	0	8.5	$6.5 \cdot 10^{-3}$	815 R	CS str., s., I, III and II, IV, oph.
ν_{87}	B_1	797	5.8	0	0	809 IR	I–IV benz. ring. sw., ip., ct., A, B, C, D thph. def. as.
ν_{86}	A	792	0	264.4	$2.1 \cdot 10^{-1}$	742 R	Ct. bre.
ν_{84}	B_2	735	29.5	1.2	$1.1 \cdot 10^{-3}$	736 IR	II, IV benz. ring sw., ip., I, III benz. half ring def., op., ct. def. as. ip., COC bend.
ν_{83}	B_3	735	29.5	1.2	$1.1 \cdot 10^{-3}$	736 IR	I, III benz. ring sw., ip., II, IV benz. half ring def., op., ct. def. as. ip., COC bend.
ν_{82}	B_3	729	13.6	0.1	$8.9 \cdot 10^{-5}$	736 IR	I, III benz. ring sw., ip., II, IV benz. half ring def., op., ct. def., as., COC bend.
ν_{81}	B_2	729	13.6	0.1	$8.9 \cdot 10^{-5}$	736 IR	II, IV benz. ring sw., I, III benz. half ring def., op., ct. def., as., ip., COC bend.
ν_{80}	A	722	0	27.1	$2.4 \cdot 10^{-2}$		CSC bend., iph., I, III and II, IV benz. half ring def., op., ct. bre., COC bend.

Abbreviations: Exp., experimental; num., mode number; Sym., symmetry of mode; Fre., frequency, cm^{-1}; I_{IR}, IR intensity, km/mol; S_i, Raman activity, $Å^4$/amu; I_i, relative Raman intensity; def., deformation; bre., breathing; s., symmetrical vibrations; as., asymmetrical vibrations; iph., in phase vibrations; oph., out-of-phase vibration; I, II, III, IV, benzene ring numbers (Fig. 2); bend., bending; sw., swinging; rock., rocking vibrations; thph., thiophene; ct., octatetraene circle, str., stretching; ip., in plane vibration; op., out-of-plane vibration.

band 1437 cm^{-1} in the experimental Raman spectra of **TTC** molecule (Fig. 7, Table 2, ν_{147} of the *A* symmetry and ν_{145} of the B_1 symmetry) and **TSC** molecule (Fig. 8 and Table 3, ν_{146} and ν_{144}) consists only from the CH_3 symmetric deformation vibrations and therefore has no shift in **TSC** in comparison with **TTC** spectrum.

We have concluded as a general rule that the CH_3 symmetric deformation vibrational modes contain a larger contribution from the C=C asymmetric stretching vibrations of benzene rings in the IR and Raman spectra of **TSC** demonstrating a low-frequency shift in comparison with **TTC.**

Rocking CH_3 vibrations were calculated in the range 1242–835 cm^{-1} in **TTC** (Table 2) and 1232–790 cm^{-1} – in the **TSC** molecule (Table 3). In the region 1211–1147 cm^{-1} (1189–1146 cm^{-1} – in **TSC**) they are not mixed with other types of vibrations. The corresponding bands of weak intensity in the experimental infrared spectra of **TTC** and **TSC** are observed at 1206, 1165 cm^{-1} (Fig. 5) and 1223, 1160 cm^{-1} (Fig. 6), respectively. In the Raman spectra the rocking CH_3 vibrations provide the bands 1168, 1159, 1153 (a shoulder), 1136 cm^{-1} (**TTC**) and 1190, 1176, 1159, 1150, 1136 (a shoulder) cm^{-1} in **TSC** (Figs. 7 and 8, respectively).

The rocking vibrations also contribute to the C–O stretching vibrations, C–S (C–Se) stretching vibrations and other types of vibrations (Tables 2 and 3). The CH_3 torsional and twisting vibrations were calculated below 291 cm^{-1}. In the IR and Raman spectra the CH_3 torsional and twisting deformation bands are very weak (Tables S1 and S2 in Supplementary materials).

3.2.1.2. The C–O skeletal vibrations. The $\nu(C_{benz}–O)$ vibrations of the B_1 symmetry were calculated in this work as occurring at 1135 cm^{-1} in the **TTC** molecule and 1123 cm^{-1} – in the **TSC** molecule (Tables 2 and 3, ν_{106}). In the experimental IR spectrum of **TSC** they make contributions to the shoulder at 1101 cm^{-1}; in the IR spectrum of the **TTC** compound the $\nu(C_{benz}–O)$ vibrations have zero intensity. In the experimental Raman spectra of **TTC** and **TSC** compounds they contribute to the weak bands 1125 cm^{-1} (Fig. 7) and 1119 cm^{-1} (Fig. 8), respectively.

Skeletal vibrations O–CH_3 occur in the range 1055–890 cm^{-1} in the **TTC** (1048–864 cm^{-1} – in the **TSC** molecule); a series of bands 1056, 1029, 958, 917 cm^{-1} corresponds to them in the experimental IR absorption (Fig. 5) for the **TTC** compound (for the **TSC** compound they occur at 1046, 1013, 952, 883 cm^{-1}; Fig. 6). The O–CH_3 skeletal vibrations are frequently mixed with CH_3 rocking and C–S (C–Se) stretching vibrations (Tables 2 and 3). The IR absorption intensity of the O–CH_3 stretching vibrations at 1056 cm^{-1} in **TTC** (Fig. 5) and 1046 cm^{-1} in **TSC** (Fig. 6) is very strong. At the same time the skeletal O–CH_3 vibrations are weak in the Raman spectra (Tables 2 and 3).

Bending vibrations of the C_{benz}–O–CH_3 angles of methoxy substituents in IR spectrum of the **TTC** molecule are calculated in the range 735–399 cm^{-1} (Table S1) and in the range 749–387 cm^{-1} – in the **TSC** molecule (Table S2). In the calculated IR spectrum of the **TTC** compound the contribution of the C_{benz}–O–CH_3 bending angle vibrations to the weak bands at 460 and 735 cm^{-1} occurs (exp.: 736 cm^{-1}, Fig. 5); in the **TSC** spectrum these are at 414, 698 and 749 cm^{-1} (exp.: 763 cm^{-1}, Fig. 6). Experimentally observed bands are the terminal features in the extreme of the spectra (Figs. 5 and 6). In the Raman spectrum of the **TTC** the bending vibrations of the C_{benz}–O–C angles produce a very weak band 722 cm^{-1} (Table 2, ν_{80}), and a weak band 736 cm^{-1} in the Raman spectrum of **TSC** (Table 3, ν_{82}). These vibrations provides out-of-plane deformations in benzene half rings (Tables S1 and S2).

In general, among all C–O modes only the O–CH_3 skeletal vibrations are very active in IR spectra providing the strongest feature, 1056 and 1046 cm^{-1}, in **TTC** and **TSC** molecules, respectively. This frequency shift and large IR absorption intensity indicate the complicated nature of such modes (various combinations of the polarized C–O modes and also the cycle distortion).

3.2.2. Ring vibrations

3.2.2.1. The benzene fragments C=C stretching vibrations. The IR bands of the skeleton vibrations of the aromatic C=C bonds are usually observed in the region 1625–1430 cm^{-1} [57]. Since the permanent dipole moment of the benzene molecule is equal to zero, only asymmetric C=C vibrations are allowed in its IR spectrum (E_{1u} vibrations) (exp.: 1484 cm^{-1} (gas phase) [58], 1479 cm^{-1} (in condensed phase) official web site of National Institute of Advanced Industrial Science and (AIST) [59]). In the IR spectrum of the **TTC** molecule which contains four condensed benzene rings these vibrations are split, mixed with other types of vibrations and give rise to three bands of medium-to-strong intensity with the calculated frequencies 1452, 1418 and 1242 cm^{-1} (quasidegenerate normal modes $\nu_{149(148)}$, $\nu_{141(140)}$ and $\nu_{130(129)}$, respectively, Table 2). In the experimental IR spectrum of **TTC** we observe a well distinguished absorption at 1420 cm^{-1} and very strong bands at 1459 and 1264 cm^{-1} (Fig. 5); they being correspond to the ν_{as}(C=C) type. In the IR spectrum of the **TSC** molecule (Table 3, Fig. 6) the calculated (1447, 1408 and 1231 cm^{-1}) and experimental frequencies (1445, 1409 and 1246 cm^{-1}) of asymmetric C=C vibrations are slightly shifted into the low-frequency region in comparison with the **TTC** molecule.

Table 3
*Calculated and experimental vibrational modes of tetraselena[8]circulene.

Nu.	Sym.	Fre.	I_{IR}	S_i	I_i	Exp.	Assignment
ν_{198}	A	2978	0	411.5	$5.9 \cdot 10^{-2}$		CH_3 str., as., I, III
ν_{197}	B_2	2978	53.0	7.3	$1.1 \cdot 10^{-3}$	2970 IR	CH_3 str., as., I, III
ν_{196}	B_3	2978	24.8	51.9	$7.5 \cdot 10^{-3}$		CH_3 str., as., I, III
ν_{195}	B_1	2978	10.8	295.5	$4.3 \cdot 10^{-2}$		CH_3 str., as., I, III
ν_{194}	A	2978	0	361.4	$5.2 \cdot 10^{-2}$		CH_3 str., as., II, IV
ν_{193}	B_3	2978	55.7	6.3	$9.2 \cdot 10^{-4}$	2970 IR	CH_3 str., as., II, IV
ν_{189}	B_2	2943	69.1	57.2	$8.4 \cdot 10^{-3}$	2941 IR	CH_3 str., as., I, III
ν_{185}	B_3	2940	59.5	0.005	$7.1 \cdot 10^{-7}$	2941 IR	CH_3 str., as., II, IV
ν_{182}	A	2875	0	798.0	$1.2 \cdot 10^{-1}$		CH_3 str., s., I, III iph.
ν_{181}	B_2	2875	138.2	10.5	$1.6 \cdot 10^{-3}$	2876 IR	CH_3 str., s., I, III oph.
ν_{178}	A	2872	0	553.4	$8.4 \cdot 10^{-2}$		CH_3 str., s., II, IV iph.
ν_{177}	B_3	2872	138.9	4.5	$6.9 \cdot 10^{-4}$	2876 IR	CH_3 str., s., II, IV oph.
ν_{176}	B_1	2872	125.3	1.9	$2.9 \cdot 10^{-4}$	2876 IR	CH_3 str., s., II oph. and IV oph.
ν_{173}	B_3	1558	145.2	7.8	$2.7 \cdot 10^{-3}$	1576 IR	CC str., s., II, IV oph.
ν_{172}	B_2	1558	137.4	0.004	$1.5 \cdot 10^{-6}$	1576 IR	CC str., s., I, III oph.
ν_{171}	A	1555	0	1534.3	$5.2 \cdot 10^{-1}$	1572 R	CC str., s., I–IV iph.
ν_{170}	B_1	1548	14.9	129.6	$4.4 \cdot 10^{-2}$	1563 R	CC str., s., I, III oph., II, IV oph., $C^{\alpha}C^{\beta}$ and $C^{\alpha'}C^{\beta'}$ str., as., A, B, C, D
ν_{169}	B_1	1546	3.5	1365.6	$4.7 \cdot 10^{-1}$	1547 R	CC str., s., I–IV, $C^{\alpha}C^{\beta}$ and $C^{\alpha'}C^{\beta'}$ str., s., CSeC bend., A, C iph. and B, D, iph.
ν_{168}	B_2	1545	1.7	32.3	$1.1 \cdot 10^{-2}$	1534 R	CC str., s., II, IV iph.
ν_{167}	B_3	1544	13.2	0	0		CC str., s., I, III iph.
ν_{166}	A	1482	0	31.6	$1.1 \cdot 10^{-2}$	1496 R	CH_3 bend, as., II, IV
ν_{165}	B_3	1482	41.5	6.6	$2.4 \cdot 10^{-3}$	1496 R	CH_3 bend, as., II, IV
ν_{164}	A	1480	0	42.7	$1.5 \cdot 10^{-2}$	1482 R	CH_3 bend, as., I, III
ν_{163}	B_2	1480	26.0	0.05	$1.9 \cdot 10^{-5}$		CH_3 bend, as., I, III
ν_{161}	B_1	1475	0.05	8.7	$3.1 \cdot 10^{-3}$	1479 R	CH_3 bend, as., II, IV
ν_{159}	B_1	1473	4.0	11.8	$4.3 \cdot 10^{-3}$	1474 R	CH_3 bend, as., I, III
ν_{158}	A	1460	0	139.8	$5.1 \cdot 10^{-2}$	1463 R	CH_3 bend, as., I–IV
ν_{157}	B_3	1460	1.8	8.3	$3.0 \cdot 10^{-3}$	1463 R	CH_3 bend, as., II, IV
ν_{155}	A	1459	0	29.5	$1.1 \cdot 10^{-2}$	1463 R	CH_3 bend, as., I–IV
ν_{154}	B_1	1458	9.1	22.9	$8.4 \cdot 10^{-3}$	1463 R	CH_3 bend, as., II, IV
ν_{152}	B_1	1458	0.07	19.2	$7.0 \cdot 10^{-3}$	1463 R	CH_3 bend, as., I, III
ν_{151}	B_3	1458	21.9	0.1	$3.9 \cdot 10^{-5}$		CH_3 bend, as., I, III
ν_{150}	B_3	1447	64.6	0.0007	$2.6 \cdot 10^{-7}$	1445 IR	CH_3 bend, s., II oph., IV oph., I oph., III oph., CC str., as., II, IV oph.
ν_{149}	A	1447	0	462.2	$1.7 \cdot 10^{-1}$	1447 R	CH_3 bend, s., CC str., as., I–IV oph.
ν_{148}	B_2	1446	55.2	0.03	$1.3 \cdot 10^{-5}$	1445 IR	CH_3 bend, s., I, III oph., IIoph., IV oph., CC str., as., I, III oph.
ν_{147}	B_1	1445	3.7	52.5	$1.9 \cdot 10^{-2}$	1437 R	CH_3 bend, s., II oph., IV oph.
ν_{146}	A	1444	0	138.0	$5.1 \cdot 10^{-2}$	1437 R	CH_3 bend, s., I, III iph., II, IV iph.
ν_{144}	B_1	1442	4.0	84.3	$3.1 \cdot 10^{-2}$	1437 R	CH_3 bend, s., I oph., III oph., II oph., IV oph.
ν_{142}	A	1416	0	699.4	$2.6 \cdot 10^{-1}$	1412 R	CH_3 bend, s., I–IV iph., CC str., as., I–IV iph., $C^{\alpha}C^{\beta}$, $C^{\alpha'}C^{\beta'}$ str., iph. and $C^{\beta}C^{\beta'}$ str. oph., CSC bend iph.
ν_{141}	B_3	1408	373.1	0.05	$1.7 \cdot 10^{-5}$	1409 IR	CH_3 bend, s., II, IV oph., CC str., as., II, IV
ν_{140}	B_2	1408	353.5	2.2	$8.3 \cdot 10^{-4}$	1409 IR	CH_3 bend, s., I, III oph., CC str., as., I, III
ν_{139}	A	1398	0	38.3	$1.5 \cdot 10^{-2}$	1392 R	CH_3 bend, s., I, III and II, IV oph., CC str., as., I, III and II, IV oph.
ν_{138}	B_1	1343	3.6	0.3	$1.4 \cdot 10^{-4}$	1350 IR	CC str., as., I, III oph., II, IV oph., $C^{\alpha}C^{\beta}$ and $C^{\alpha'}C^{\beta'}$ str., as., CSe str. as. A, B, C, D
ν_{137}	B_3	1303	336.2	0.3	$1.5 \cdot 10^{-4}$	1310 IR	CC str., as., Kekule, II, IV oph.
ν_{136}	B_2	1303	301.1	2.5	$1.1 \cdot 10^{-3}$	1310 IR	CC str., as., Kekule, I, III oph.
ν_{135}	A	1292	0	43.3	$1.8 \cdot 10^{-2}$	1307 R	CC str., as., Kekule, I–IV, iph.
ν_{134}	B_1	1274	13.2	286.1	$1.2 \cdot 10^{-1}$	1304 R	$C^{\beta}C^{\beta'}$ srt., A, C and B, D, oph.
ν_{133}	A	1267	0	369.3	$1.6 \cdot 10^{-1}$	1253 R	CC str., as., Kekule, I, III and II, IV, oph., $C^{\alpha}C^{\beta}$ and $C^{\alpha'}C^{\beta'}$ str., as., A, B, C, D
ν_{132}	B_3	1257	19.0	0.03	$1.1 \cdot 10^{-5}$	1262 IR	CC str., as., I, III, $C^{\beta}C^{\beta'}$ str., II, IV oph.
ν_{131}	B_2	1257	27.7	5.3	$2.3 \cdot 10^{-3}$		CC str., as., II, IV, $C^{\beta}C^{\beta'}$ str., I, III oph.
ν_{130}	B_2	1232	283.2	6.3	$2.8 \cdot 10^{-3}$	1246 IR	CC str., as., I, III oph., CH_3 rock., I–IV
ν_{129}	B_3	1231	355.8	10.1	$4.5 \cdot 10^{-3}$	1246 IR	CC str., as., II, IV oph., CH_3 rock., I–IV
ν_{128}	A	1231	0	2249.2	1.0	1253 R	$C^{\alpha}C^{\beta}$, $C^{\alpha'}C^{\beta'}$ str., iph. and $C^{\beta}C^{\beta'}$ str., oph., ct. def., s., CSe str., s., iph., CH_3 rock., I–IV
ν_{127}	B_1	1208	8.3	87.7	$4.0 \cdot 10^{-2}$	1208 R	$C^{\alpha}C^{\beta}$, $C^{\alpha'}C^{\beta'}$ str., s., CSe str., s., I, III and II, IV, oph., ct. def., as., CH_3 rock., I–IV
ν_{126}	B_2	1205	21.9	4.3	$1.9 \cdot 10^{-3}$	1223 IR	I, III benz. def. s., oph., CH_3 rock., II, IV, $C^{\alpha}C^{\beta}$, $C^{\alpha'}C^{\beta'}$ str., iph. and $C^{\beta}C^{\beta'}$ str. oph., CSe str., s.
ν_{125}	B_1	1204	29.0	36.4	$1.7 \cdot 10^{-2}$	1223 IR 1204 R	$C^{\alpha}C^{\beta}$, $C^{\alpha'}C^{\beta'}$ str., s., CSe str., s., I, III and II, IV, oph., ct. def., as., CH_3 rock., I–IV
ν_{123}	A	1189	0	15.6	$7.2 \cdot 10^{-3}$	1190 R	CH_3 rock., I–IV
ν_{122}	B_1	1185	13.6	22.5	$1.0 \cdot 10^{-2}$	1190 R	CH_3 rock., I–IV
ν_{120}	A	1182	0	170.3	$7.9 \cdot 10^{-2}$	1176 R	CH_3 rock., I–IV
ν_{117}	B_2	1157	39.1	0.02	$1.1 \cdot 10^{-5}$	1160 IR	CH_3 rock., II, IV
ν_{115}	B_1	1153	64.6	0.005	$2.4 \cdot 10^{-6}$	1160 IR	CH_3 rock., I–IV, CSe str., as.
ν_{111}	A	1149	0	15.0	$7.2 \cdot 10^{-3}$	1150 R	CH_3 rock., II, IV
ν_{108}	A	1146	0	14.1	$6.8 \cdot 10^{-3}$	1136 R	CH_3 rock., I, III
ν_{106}	B_1	1123	16.6	138.1	$6.8 \cdot 10^{-2}$	1101 IR 1119 R	C_{benz}–O str., I oph., II oph., III oph., IV oph., I–IV benz. def., as., $C^{\beta}C^{\beta'}$ str., A, C and B, D, oph., CH_3 rock., I–IV
ν_{105}	B_3	1048	501.1	4.4	$2.4 \cdot 10^{-3}$	1046 IR	H_3C–O str., I oph., III oph., II iph., IV iph., ct. sw.
ν_{104}	B_2	1047	303.4	2.3	$1.2 \cdot 10^{-3}$	1046 IR	H_3C–O str., I iph., III iph., II oph., IV oph., ct. sw.
ν_{103}	A	1032	0	31.4	$1.7 \cdot 10^{-2}$	1041 R	H_3C–O str., I–IV iph., I–IV benz. def., s., iph., CSe str., s., iph.
ν_{102}	B_2	1011	140.2	27.0	$1.5 \cdot 10^{-2}$	1013 IR 1027 R	H_3C–O str., I iph., III iph., II oph., IV oph., I, III benz. def., s., oph., ct., II, IV benz. def. as., CSe str., s.
ν_{101}	B_3	1009	8.5	5.6	$3.2 \cdot 10^{-3}$	1015 R	H_3C–O str., I oph., III oph., II iph., IV iph., II, IV benz. def., s., oph., ct., I, III benz. def. as., CSe str., s.
ν_{100}	B_1	1007	218.4	7.2	$4.1 \cdot 10^{-3}$	1013 IR 1004 R	H_3C–O str., I oph., II oph., III oph., IV oph., I–IV benz. def., as., CSe str., as.

(*continued on next page*)

Table 3 (*continued*)

Nu.	Sym.	Fre.	I_{IR}	S_i	I_i	Exp.	Assignment
ν_{99}	A	1004	0	26.5	$1.5 \cdot 10^{-2}$	992 R	H_3C–O str., I, III iph., II, IV iph., I, III and II, IV benz. def., s., oph., CSe str., as.
ν_{98}	B_1	972	0.3	11.0	$6.4 \cdot 10^{-3}$	972 R	H_3C–O str., I oph., II oph., III oph., IV oph., I–IV benz. def., as., CSeC bend., A, C and B, D oph.
ν_{97}	B_2	938	2.0	9.7	$5.9 \cdot 10^{-3}$	940 R	H_3C–O str., II oph., IV oph., II, IV benz. def., as., I, III benz. def. s., oph., CH_3 rock., II, IV
ν_{96}	B_3	936	26.3	7.4	$4.5 \cdot 10^{-3}$	952 IR 929 R	H_3C–O str., I oph., III oph., I, III benz. def. as., II, IV benz. def., s., oph., CH_3 rock., I, III
ν_{95}	A	902	0	14.7	$9.3 \cdot 10^{-3}$	905 R	H_3C–O str., I–IV iph., I, III and II, IV benz. def., s., oph., ct. def., s., CH_3 rock., I–IV, CSe str., s.
ν_{94}	B_3	883	0.2	0.5	$3.0 \cdot 10^{-4}$	859 R	H_3C–O str., II, IV oph., II, IV benz. def., s., oph., CH_3 rock., II, IV
ν_{93}	B_2	883	0.1	0.7	$4.3 \cdot 10^{-4}$	847 R	H_3C–O str., I, III oph., I, III benz. def., s., oph., CH_3 rock., I, III
ν_{92}	A	866	0	1.7	$1.1 \cdot 10^{-3}$	830 R	H_3C–O str., I, III and II, IV oph., I, III and II, IV benz. def. s., oph., CH_3 rock., I–IV, CSe str., as.
ν_{91}	B_1	864	31.1	2.0	$1.3 \cdot 10^{-3}$	883 IR 815 R	H_3C–O str., I oph., II oph., III oph., IV oph., I–IV benz., ct. def., as., CH_3 rock., I–IV, CSe str., as.
ν_{90}	B_1	792	17.7	4.4	$3.3 \cdot 10^{-3}$	777 R	CSe str., s., I, III and II, IV, oph., CH_3 rock., I–IV
ν_{89}	B_3	791	51.2	1.4	$1.1 \cdot 10^{-3}$	803 IR 768 R	CSe str., as., I–IV, displacement of I, III benz. moieties along y-direction, ct. def. as., CH_3 rock., I, III
ν_{88}	B_2	790	61.6	1.6	$1.2 \cdot 10^{-3}$	803 IR 754 R	Displacement of II, IV benz. moieties along y-direc-tion, CSe str., as., I–IV, ct. def. as., CH_3 rock., II, IV
ν_{86}	A	768	0	222.3	$1.7 \cdot 10^{-1}$	733 R	Ct. bre.
ν_{84}	B_2	749	56.0	0.5	$3.6 \cdot 10^{-4}$	763 IR	II, IV benz. ring sw., I, III benz. half ring def., op., ct. def., as., ip., COC bend.
ν_{82}	A	736	0	74.9	$6.0 \cdot 10^{-2}$		CSeC bend., iph., I, III and II, IV benz. half ring def., op., ct. bre., COC bend.

* For abbreviation description see the Table 2 capture.

In the Raman spectrum of the **TSC** the asymmetric benzene ring C=C stretching vibrations are more active in comparison with those of the **TTC** molecule. Upon mixing with other vibrations they provide contribution to the calculated bands of medium intensity 1447 cm^{-1} (exp.: 1447 cm^{-1}) and 1416 cm^{-1} (exp.: 1412 cm^{-1}) in the Raman spectrum of the **TSC** (Fig. 8) and to a weak band 1425 cm^{-1} (exp.: 1426 cm^{-1}) – in **TTC**. The late band shows the higher experimental intensity (Fig. 7).

The modes ν_{136}, ν_{135} in **TTC** molecule (calc.: 1312 cm^{-1}, exp.: 1321 cm^{-1}) and ν_{137}, ν_{136} in **TSC** molecule (calc.: 1303 cm^{-1}, exp.: 1310 cm^{-1}) indicate a strong IR intensity and belong to the skeleton vibrations of the benzene rings, which include subsequent alternations of the C=C bonds stretching and compression of a large amplitude (Kekule type vibrations). The benzene vibrations of this type (B_{2u}), calculated at 1311 cm^{-1}, are symmetry forbidden in IR and Raman spectra of benzene molecule and have never been observed. The clear appearance of this peak in the IR spectrum of **TTC** and **TSC** (Figs. 5 and 6) is an interesting manifestation of mutual atomic influence and common conjugation effect. In the Raman spectra of the **TTC** and **TSC** molecules the Kekule vibrations ν_{133} of the *A* symmetry produce the bands with moderate intensity at 1285 cm^{-1} (exp.: 1282 cm^{-1}) and 1267 cm^{-1} (exp.: 1253 cm^{-1}), respectively (Tables 2 and 3, Figs. 7 and 8). These bands of the ν_{as}(C=C) Kekule vibrations type have essential contributions of the C=C vibrations from the side of thiaphen (selenophen) moiety.

In the experimental IR spectra of the **TTC** and **TSC** compounds vibrational modes ν_{173} of the B_2 symmetry (calc.: 1571 cm^{-1}) and ν_{172} of the B_3 symmetry (calc.: 1558 cm^{-1}) correspond to a weak bands of symmetric C=C vibrations at 1580 cm^{-1} (Fig. 5) and 1576 cm^{-1} (Fig. 6), respectively. Another symmetric C=C vibrations of the B_2 and B_3 type (modes ν_{169} and ν_{168}, respectively) at 1548 cm^{-1} gives a very weak band at 1560 cm^{-1} in the IR spectrum of **TTC** molecule; the same band is not observed in the calculated and experimental IR spectra of **TSC** (Fig. 6) because of the weak intensity (Table 3, ν_{168}, ν_{167}).

Symmetric C=C vibrations of the B_1 type (modes ν_{170} and ν_{167} calculated at 1552 and 1546 cm^{-1} in the **TTC** molecule, respectively, and corresponding modes ν_{170} and ν_{169} at 1548 and 1546 cm^{-1} in **TSC** molecule, Tables 2 and 3) are very similar to the 1602 cm^{-1} vibration band in the Raman spectrum of benzene (ν_{16} according to Herzberg's numeration [58]. These modes contain appreciable contribution of stretching and bending vibrations of the thiophene (or selenophene) rings, which explain a significant frequency shift compared to benzene. The corresponding band in Raman spectrum is strong. The very intense peak in the Raman spectra of the **TTC** and **TSC** molecules (Figs. 7 and 8) is formed by a totally symmetric *A* mode ν_{171} at 1568 cm^{-1} (exp.: 1580 cm^{-1}) and 1555 cm^{-1} (exp.: 1572 cm^{-1}), respectively. The band 1555 cm^{-1} in the calculated Raman spectra of **TSC** (Fig. 8) overlaps the strong band 1546 cm^{-1}, which has besides the symmetric C=C vibrations a contribution of stretching and bending vibrations of the selenophene moiety. In the experimental Raman spectrum of the **TSC** compounds there are two bands (1572 and 1547 cm^{-1}). The same bands in the calculated **TTC** spectrum do not overlap each other (Fig. 8, curve 1).

In a free benzene molecule the most of C=C vibrations are symmetry forbidden by the selection rules for IR and Raman activity. But in the **TTC** and **TSC** compounds the benzene moieties are clearly perturbed by the common π-conjugation effect and the initially forbidden benzene C=C modes are getting allowed because of the symmetry distortion. Appearance of the numerous C=C vibrations of benzene fragments both active in the finger-print region of the **TTC** and **TSC** IR and Raman spectra illustrates the important fundamental properties of the tetrathia[8]circulene and tetraselena[8]circulene π-extended system. The non-zero intensity of the corresponding bands in the observed IR absorption and Raman scattering of the studied molecules being in a good agreement with DFT calculations provides a clear assignment of the molecular force field and correct interpretation of all the vibrational modes. In fact these vibrational features are more informative than the small structural changes, presented in Table 1, in respect to comprehensive understanding of electronic structure peculiarities in the large family of tetraX[8]circulene compounds (X = oxa, thia, selena).

3.2.2.2. Thiophene and selenophene related ring vibrations. Symmetric vibration of the $C^{\alpha}C^{\beta}$ bonds mixed with the out-of-phase vibration of the $C^{\beta}C^{\beta'}$ bond of the A_1 symmetry (C_{2v} point group) which is active in both IR and Raman spectra have been calculated at 1414 cm^{-1} (exp.: 1410 and 1408 cm^{-1} from IR vapor and Raman liquid, respectively [60] for the free thiophene and at 1429 cm^{-1} – for the free selenophene molecules (exp.: 1423, 1421 and 1419 cm^{-1} from IR vapor, IR liquid and IR of solid, respectively [60]. This vibration is splitted into the four corresponding modes in the calculated vibrational spectra of the **TTC** and **TSC** molecules: *A* modes ν_{142}, ν_{128}, B_2 mode ν_{126} and B_3 mode ν_{125} (in **TSC** – ν_{124}), Tables 2 and 3) and responsible for the most intense line 1241 cm^{-1} and weak line 1425 cm^{-1} in the

calculated Raman spectra of **TTC** (Fig. 7), 1231 and 1416 cm^{-1}, respectively, – in **TSC** (Fig. 8). The most intense line has some symmetric CX stretching vibration contribution, the weak line – CXC bending contribution (X = thia, selena). These B_2 and B_3 modes give a contribution into the very weak band at 1211 cm^{-1} (exp.: 1206 cm^{-1}) and 1204 cm^{-1} (exp.: 1223 cm^{-1}) in the IR spectrum of **TTC** and **TSC**, respectively (Figs. 5 and 6).

Asymmetric vibrations of the $C^{\alpha}C^{\beta}$ bonds of the B_2 symmetry (molecule in the yz plane) are allowed in both IR and Raman spectra of thiophene and selenophene and calculated for the free thiophene molecule at 1520 cm^{-1}, at 1528 cm^{-1} – for the selenophene molecule. The corresponding bands in the calculated IR spectra of the thiophene and selenophene molecules are not observed because of they are too weak. This type of vibrations in **TTC** and **TSC** molecules mixed up with the vibrations benzene fragments of the C=C bonds. In the IR spectrum of **TTC** molecule the normal modes ν_{167} and ν_{138} of the B_1 symmetry with a frequencies of 1546 and 1354 cm^{-1}, respectively, corresponds to the mixed stretching vibrations of the C=C bonds in the benzene and thiophene fragments and are not observed because they are too weak. In the IR spectrum of **TSC** molecule these vibrations correspond to the normal modes ν_{170} and ν_{138} with the calculated frequencies of 1548 and 1343 cm^{-1} (Table 3). In the calculated Raman spectra of the **TTC** (Fig. 7) and **TSC** molecule (Fig. 8), the bands of the weak intensity is due ν_{133} normal mode of the *A* symmetry with a frequencies of 1285 cm^{-1} (exp.: 1282 cm^{-1}) and 1267 cm^{-1} (1253 cm^{-1}), respectively, which corresponds to mixed asymmetric stretching vibrations of the C=C bonds in the benzene and thiophene (selenophene) fragments.

The C–S and C–Se bonds stretching vibrations have been calculated for the free thiophene and selenophene molecules in the following regions (comparing with the experimental IR spectra [57] measured in a gas phase): ν_s(C–S) = 818 cm^{-1} (exp.: 839 cm^{-1}) and ν_{as}(C–S) = 730 cm^{-1} (exp.: 751 cm^{-1}), ν_s(C–Se) = 749 cm^{-1} and ν_{as}(C–Se) = 608 cm^{-1} (exp.: 755 cm^{-1} and 626 cm^{-1}, respectively). The frequencies of normal modes contributing to the stretching vibrations ν(C–S) and ν(C–Se) in the IR and Raman spectra of the **TTC** and **TSC** molecules are calculated in the region 1354–840 cm^{-1} and 1343–790 cm^{-1}, respectively (Tables 2 and 3). Since upon the formation of circulene macrocycle the C–S and C–Se bond lengths remain almost invariable (Table 1), we assume that the calculated ring stretching vibrations are induced mainly with the skeletal macrocycle deformations and the substituents vibrations.

The bending CXC vibrations (X = S, Se) of the A_1 symmetry are calculated for the free thiophene and selenophene molecules at 601 and 450 cm^{-1}, respectively and active in the Raman spectrum. Upon the macrocycle formation the C–S–C angle degreases on 2.7° (from 91.5° to 88.8°), and C–Se–C angle decreases on 3.4° (from 87.0° to 83.6°), which provides frequency increasing for the δ(CXC) vibrations up 656 cm^{-1} for the **TTC** molecule (ν_{79}) and 593 cm^{-1} for the **TSC** molecule (ν_{70}). The corresponding bands in the IR and Raman spectra are not observed because they were too weak.

3.2.2.3. Rings deformation vibrations. The planar skeleton rings deformations have been calculated at lower frequencies than 1241 cm^{-1} in **TTC** molecule and 1231 cm^{-1} in **TSC** molecule. These modes consist of contribution from the symmetric or asymmetric stretching vibrations, ring breathing and most of them additionally mixed with other types of vibrations – ν($C^{\alpha}C^{\beta}$), ν(OCH_3), ν(CS) (ν(CSe)) or with the δ(CSC) (δ(CSeC)), δ($C_{benz}OCH_3$) angles. For the **TTC** molecule we have predicted in-phase breathing of all rings at the frequence 258 cm^{-1} (Table S1, ν_{40}) and at 214 cm^{-1} for the **TSC** molecule (Table S2, ν_{37}). The inner octatetraene ring breathing calculated at 792 cm^{-1} (ν_{86}), 722 cm^{-1} (ν_{80}) for the **TTC** molecule and at 768 (ν_{86}), 736 cm^{-1} (ν_{82}) for the **TSC** molecule but all these modes are forbidden in IR absorption however allowed in the Raman scattering (Tables 2 and 3). The experimental bands 742 and 733 cm^{-1} in the Raman spectra of the **TTC** (Fig. 7) and **TSC** (Fig. 8) compounds, respectively, correspond to the breathing vibrations of the octatetraene ring, but the calculated and observed frequencies are rather different (up to 50 cm^{-1} in **TTC**); this is the largest deviation across all spectra. The octatetraene ring breathing is a particular vibration and its force field is difficult to reproduce.

Symmetric and asymmetric in-plane deformations of the benzene fragments make a contribution into the very weak experimental IR bands at 1206, 958, 917 cm^{-1} and into the moderately intensive band at 1029 cm^{-1} **TTC** molecule (Fig. 5, curve 2). In IR spectrum of the **TSC** molecule to them correspond the bands 1223, 952, 883 and 1013 cm^{-1} (Fig. 6, curve 2). Out-of-plane half ring deformations of benzene fragments and asymmetric in-plane deformations of the octatetraene ring make a contribution to the very weak experimental bands 736 cm^{-1} and 763 cm^{-1} in the IR spectra of the **TTC** and **TSC** molecules, respectively (Figs. 5 and 6).

In general, we can conclude that our DFT calculations explain well all visible features in experimental vibrational spectra which is useful for the future investigation of the vibronic effects in the **TTC** and **TSC** absorption and emission electronic spectra.

3.3. UV–vis spectra of *TTC* and *TSC*

The experimentally detected UV–vis spectra [43] of tetrathia[8]circulene 18 and tetraselena[8]circulene 19 are presented in Fig. 9 (blue lines). As one can see from Fig. 9 the experimental UV–vis absorption spectra of the both **TTC** and **TSC** molecules consist of the long-wavelength absorption band in the region 320–450 nm and the short-wavelength absorption bands in the UVB region. The experimentally measured UV–vis spectra of **TTC** and **TSC** are well reproduced by our TD DFT/B3LYP/6-311++G(d,p) calculation (Fig. 9, red curves) which provides an opportunity to assign the nature of all experimentally observed absorption bands (Table 4).

For the both studied **TTC** and **TSC** molecules the first electronic transition into the S_1 excited state (Table 4) is symmetry allowed but it has very weak intensity in the electric dipole approximation which corresponds to the weak fluorescence intensity [43]. It is interesting that for the **TTC** molecule the fluorescence intensity is relatively stronger than for the **TSC** species in a good qualitative agreement with the calculated oscillator strengths for the $S_0 \rightarrow S_1$ electronic transition (Table 4). We have supposed that the $S_0 \rightarrow S_1$ transition produces the vibronic 0–1 satellite at about 403 nm in absorption spectrum of **TTC** which clearly seen in the form of a shoulder at the right side of the 391 nm absorption band (Fig. 9, blue line). This fact explains the well observed vibronic structure in the **TTC** fluorescence spectrum (Fig. 4 in Ref. [43] in a contrast with the single-band fluorescence of **TSC** for which the $S_0 \rightarrow S_1$ is not vibronically-active in both absorption and fluorescence spectra [43]. The second and third electronic transitions into the quasidegenerate 1^1B_3 and 1^1B_2 excited states (Table 4) provide the strong bands at 391 and 411 nm in the experimental spectra of **TTC** and **TSC** compounds, respectively. There are also the 0–1 vibronic bands (corresponding maxima at 373 and 391 nm). In the absorption spectrum of **TTC** even the very weak 0–2 vibronic satellite is clearly seen (Fig. 9 and Table 4).

The short-wavelength absorption in the experimental spectrum of **TTC** compound consists of two bands with the maxima at 294 and 261 nm. According to our TD DFT/B3LYP/6-311++G(d,p) calculations the former band (294 nm) corresponds to the double electronic transitions into the 3^1B_3 and 3^1B_2 excited states (Table 4). The low-lying electronic transitions into the 2^1B_3 and 2^1B_2 excited

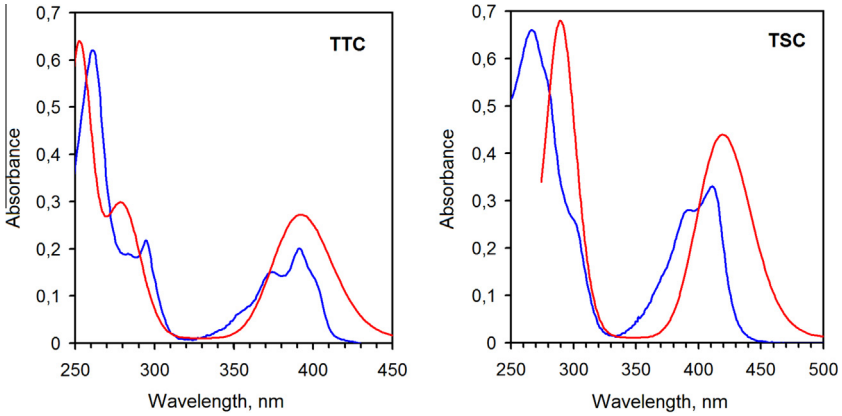

Fig. 9. UV–vis absorption spectra of **TTC** and **TSC** compounds: blue lines – experimental spectra measured in CH_2Cl_2 solution, red lines – TD DFT/B3LYP/6-311++G(d,p) calculated spectra tacking into account the PCM solvation model (solvent – CH_2Cl_2). (For interpretation of the references to color in this figure legend, the reader is referred to the web version of this article.)

states are overlapped by the $S_0 \rightarrow S_{13}$, S_{14} transitions (Table 4) resulting in the total band maximum at 279 nm. The band at 261 nm can be assigned to the $X^1A \rightarrow 7^1B_3$ and $X^1A \rightarrow 7^1B_2$ transitions which have relatively high oscillator strengths. All the discussed $X^1A \rightarrow N^1B_3$ and $X^1A \rightarrow N^1B_3$ transitions are polarized along the X and Y axis, respectively (Fig. 4) and correspond to $\pi \rightarrow \pi^*$ excitations (selected MOs are presented in Fig. 10). We should note that the degeneracy of the B_2 and B_3 electronic states in the **TTC** spectrum is accidental, i.e. these states are not strictly degenerate in the framework of the D_2 symmetry point group. The **TTC** molecule is almost planar and its symmetry is close to the D_{4h} point group in which B_2 and B_3 states should transform into the strictly doubly degenerated E_u states [25,33]. On the other hand, **TSC** molecule is significantly bent, i.e. its geometry differs from the planar D_{4h} symmetry in a large extend. This fact provides the perceptible splitting of the B_2 and B_3 states in the calculated **TSC** spectrum both by the energy and intensity (Table 4).

Similarly to the **TTC** compound, the experimental absorption spectrum of **TSC** consists of the intense band at 267 nm with the right-side shoulder at about 301 nm. The calculated absorption spectrum of **TSC** consists of only single band (289 nm) which corresponds to the experimental maximum at 267 nm. By this way the shoulder at about 301 nm can be assigned to the $X^1A \rightarrow 2^1B_3$ and $X^1A \rightarrow 2^1B_2$ electronic transitions both calculated at 300 nm (Table 4). However in the simulated spectrum they are completely overlapped by the main band at 289 nm and do not produce a separate band or shoulder.

One should note that many calculated low-intensity transitions are omitted in Table 4, since they are overlapped in the simulated spectrum (Fig. 9).

*3.4. Aromaticity of the **TTC** and **TSC** molecules and their doubly charged ions*

During last few years there are numerous works devoted to the study of hetero[8]circulenes aromaticity [16,17,27,29,61–63]. However, all the studies are reduced to one common conclusion: all planar hetero[8]circulenes possess the diatropic (“aromatic”) ring currents in the outer perimeter and the paratropic (“antiaromatic”) ring currents in the inner eigth-member core. We have recently shown [29] that the total magnetically-induced ring current of the planar hetero[8]circulenes is equal almost zero, i.e. these compounds represent the unusual bifacial conjunction of aromatic and antiaromatic magnetic evidences. On the other hand, the double ionization of the hetero[8]circulenes usually leads to unexpected results [10,16,17,29] and particularly provides the drastic changes of the balance between the diatropic and paratropic ring currents. The **TTC** and **TSC** molecules are not an exception. The inner octatetraene core of the neutral **TTC** and **TSC** species is characterized by the positive NICS(0) values (Fig. 11) which correspond to the presence of the paratropic ring currents, i.e. indicate the antiaromaticity of these cores. The significantly negative NICS(0) values at the center of the benzene, thiophene and selenophene rings for **TTC** and **TSC** neutral compounds (Fig. 11) indicate the presence of magnetically-induced diatropic ring current, i.e. the aromatic character of these rings. In this way, the neutral hetero[8]circulenes are predicted to be almost non-aromatic compounds in the framework of the magnetic ring-current criterion because of paratropic and diatropic ring-current should be completely compensated yielding almost zero net current similarly to tetraoxa[8]circulenes [29], azaoxa[8]-circulenes [29], fullerene C_{60} [64], etc.

In contrast to neutral molecules, the dianionic **TTC** and **TSC** species are found to be a completely aromatic because of the inner octatetraene core and all the surrounding benzene, thiophene and selenophene moieties are strongly aromatic (the corresponding NICS(0) indexes are significantly negative, Fig. 11). From the other hand the dicationic **TTC** and **TSC** species are predicted to possess a strongly antiaromatic octatetraene core, but the other benzene, thiophene and selenophene rings still support an aromatic character (Fig. 11). So, despite the slightly unplanar conformation of the **TTC** and **TSC** neutral molecules and related doubly charged ions demonstrate the similar electronic structure and ring current peculiarities like the other planar hetero[8]circulenes and their doubly charged ions.

4. Experimental section

4.1. FT-IR spectra

Fourier transform infrared (FT-IR) spectra were recorded in transmission mode using a Nicolet 5700 spectrometer coupled to a Continuum XL (Thermo Scientific, Nicolet, USA) microscope. The solid samples were put in the center of KBr tablets. The infrared microscope was equipped with a liquid nitrogen cooled mercury cadmium telluride MCT/A detector. Infrared spectra were collected between 500 and 4000 cm^{-1} with a resolution of 4 cm^{-1}.

4.2. Resonance Raman experiments

Resonance Raman experiments were performed for **TTC** and **TSC** in CH_2Cl_2 solvent. The 10 ml solutions were studied in a flowing jet

Table 4
Wavelengths (λ), oscillator strengths (f) and orbital assignment of the selected electronic transitions in the calculated absorption spectra of **TTC** and **TSC** compounds.

State	Transition	λ_{calc} (nm)	λ_{exp} (nm)	f	Assignment
TTC					
T_1	$X^1A \rightarrow 1^3B_1$	515		0	HOMO-2 → LUMO (85%)
S_1	$X^1A \rightarrow 1^1B_1$	414	422 (0–0) 403 (0–1)	0.0011	HOMO-2 → LUMO (99%)
S_2	$X^1A \rightarrow 1^1B_2$	392	391 (0–0) 373 (0–1) 355 (0–2)	0.377	HOMO → LUMO (96%)
S_3	$X^1A \rightarrow 1^1B_3$	392		0.377	HOMO-1 → LUMO (96%)
S_8	$X^1A \rightarrow 2^1B_2$	285	294	0.207	HOMO-2 → LUMO + 1 (71%)
S_9	$X^1A \rightarrow 2^1B_3$	285		0.207	HOMO-2 → LUMO + 2 (71%)
S_{13}	$X^1A \rightarrow 3^1B_2$	275		0.260	HOMO-3 → LUMO + 1 (76%)
S_{14}	$X^1A \rightarrow 3^1B_3$	275		0.260	HOMO-3 → LUMO + 2 (76%)
S_{26}	$X^1A \rightarrow 7^1B_2$	252	261	0.811	HOMO → LUMO + 4 (62%)
S_{27}	$X^1A \rightarrow 7^1B_3$	252		0.813	HOMO-1 → LUMO + 4 (62%)
TSC					
T_1	$X^1A \rightarrow 1^3B_1$	556		0	HOMO-2 → LUMO (87%)
S_1	$X^1A \rightarrow 1^1B_1$	442		0.0009	HOMO-2 → LUMO (99%)
S_2	$X^1A \rightarrow 1^1B_3$	420	411 (0–0) 391 (0–1)	0.346	HOMO → LUMO (97%)
S_3	$X^1A \rightarrow 1^1B_2$	419		0.335	HOMO-1 → LUMO (97%)
S_9	$X^1A \rightarrow 2^1B_3$	300	301	0.139	HOMO-2 → LUMO + 1 (61%)
S_{10}	$X^1A \rightarrow 2^1B_2$	300		0.107	HOMO-2 → LUMO + 2 (55%)
S_{15}	$X^1A \rightarrow 4^1B_2$	289	267	0.330	HOMO → LUMO + 3 (48%) HOMO-2 → LUMO + 2 (36%)
S_{16}	$X^1A \rightarrow 4^1B_3$	288		0.331	HOMO-1 → LUMO + 3 (50%) HOMO-2 → LUMO + 1 (31%)

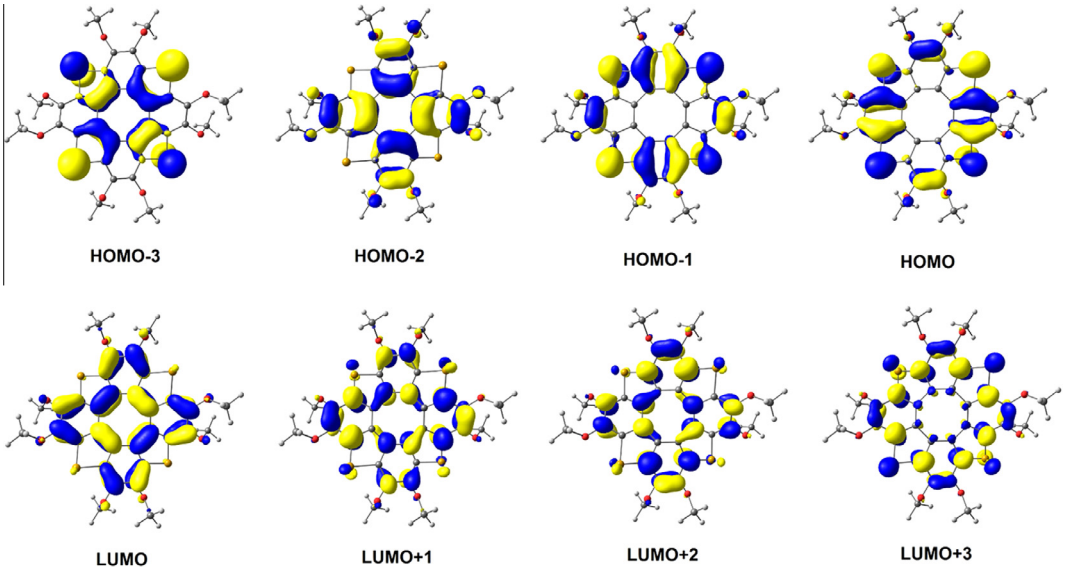

Fig. 10. The shape of selected molecular orbitals of the **TTC** and **TSC** compounds (controlling value of the isosurface is 0.03 a.u.). There is no difference between the presented MOs for both compounds.

system with an absorbance of 1 at 267 nm when used 2 mm path-length cuvette throughout the data acquisition. The resonance Raman experimental apparatus and methods used for these experiments have been described elsewhere [65,66], and only a brief description will be given here. The resonance Raman experiments were conducted using 266 nm excitation (the fourth harmonic from a Nd:YAG laser) with about 1 mW laser power. The excitation laser beam was focused to about a 0.5 mm diameter spot size onto a flowing liquid stream of sample. A backscattering geometry was employed for sample excitation and for collection of the Raman scattered light by reflective optics. The Raman signal detected by a liquid-nitrogen-cooled charged-coupled device (CCD) detector was acquired for 30 s before being read out to an interfaced personal computer, and 10 of these readouts were averaged to obtain the resonance Raman spectrum. The Raman bands of the MeCN solvent were employed to calibrate the resonance Raman spectra with an estimated accuracy of 5 cm^{-1} in absolute frequency. The Raman spectrum of the sample was obtained by removing the Raman spectrum of the corresponding solvent with a proper scaling factor.

4.3. UV–vis spectra

The UV–vis absorption spectra of **TTC** and **TSC** compounds ($c = 10^{-5}$ M) were recorded on a Varian CARY 1E UV–vis spectrophotometer in the dichloromethane solution.

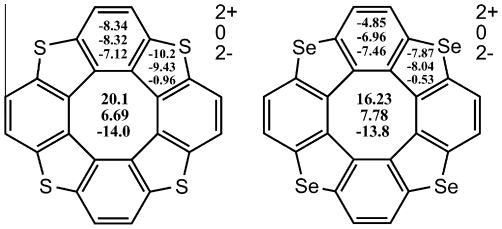

Fig. 11. The NICS(0) indexes for the neutral tetrathia[8]circulene (**TTC**) and tetraselena[8]circulene (**TSC**) and their doubly charged ions calculated by the GIAO/B3LYP/6-311++G(d,p) method (OMe substituents omitted for clarify). The top value inside the ring corresponds to the dication species, the middle value – to the neutral molecule, the bottom value – to the dianion species.

5. Conclusions

The detailed analysis of IR, Raman and UV–vis spectra calculated by DFT and TD DFT methods permit us to complete a thorough identification of these species. Comparison with the previously investigated tetraoxa[8]circulene compounds [16,17,29–34] indicates many common features in the force field and its spectral manifestations. In the Raman and IR spectra of benzene molecule a number of vibration modes are forbidden by the symmetry selection rules. But in the **TTC** and **TSC** compounds the benzene moieties are involved into the common π-conjugation chain with [8]circulene; thus the formally forbidden benzene modes are well seen and identified. Appearance of numerous vibrations of benzene fragments (like Kekule modes) being active in the finger-print region of the studied molecules in both IR and Raman spectra is confirmed by DFT calculations; this illustrates the important fundamental properties of the tetraX[8]circulene π-extended system (X = O, S, Se) in agreement with previous studies [30–34]. Analysis of the observed IR absorption and Raman scattering spectra of the studied molecules based on DFT calculations provides a clear assignment of the molecular force field and correct interpretation of all vibrational modes being consistent with the structure peculiarities in the large family of tetraX[8]circulene compounds (X = oxa, thia, selena) and their structural differences for various X.

The first $S_0 \rightarrow S_1$ electronic transition for the **TTC** and **TSC** molecules is symmetry allowed and is characterized by the non-zero oscillator strength in a great contrast to the symmetry forbidden $S_0 \rightarrow S_1$ transition of the isoelectronic tetraoxa[8]circulene. At the same time, the shape of the main long-wavelength absorption band and its vibronic structure are quite similar for both **TTC** and **TSC** molecules and for the parent tetraoxa[8]circulene because of the fundamental analogy between the B_2, B_3 quasidegenerate states (D_2 point group) and strictly degenerate $2E_u$ states (D_{4h} point group) which are produced the main long-wavelength band.

The NICS characterisation of the studied tetrathia[8]circulene and tetraselena[8]circulene molecules suggests their bifacial aromatic/antiaromatic nature: both diatropic and paratropic components exist simultaneously providing the net magnetic current close to zero like it was early established for the planar isoelectronic tetraoxa[8]circulene and related azaoxa[8]circulenes [29].

Acknowledgments

This work was supported by the Ministry of Education and Science of Ukraine Research Fund (Grant No. 0113U001694). We thank Professor Hans Ågren (KTH, Stockholm) for the PDC supercomputer use. All calculations were performed with resources provided by the Swedish National Infrastructure for Computing (SNIC) at the Parallel Computer Center (PDC) through the project "Multiphysics Modeling of Molecular Materials", SNIC 020/11-23.

Appendix A. Supplementary data

Supplementary data associated with this article can be found, in the online version, at http://dx.doi.org/10.1016/j.saa.2015.06.020.

References

[1] W. Jiang, Y. Li, Z. Wang, Chem. Soc. Rev. 42 (2013) 6113–6127.
[2] M. Iyoda, J. Yamakawa, M.J. Rahman, Angew. Chem. Int. Ed. 50 (2011) 10522–10553.
[3] A. Pron, P. Gawrys, M. Zagorska, D. Djurado, R. Demadrille, Chem. Soc. Rev. 39 (2010) 2577–2632.
[4] B. Minaev, G. Baryshnikov, H. Agren, Phys. Chem. Chem. Phys. 16 (2014) 1719–1758.
[5] C.B. Nielsen, T. Brock-Nannestad, T.K. Reenberg, P. Hammershøj, J.B. Christensen, J.W. Stouwdam, M. Pittelkow, Chem. Eur. J. 16 (2010) 13030–13034.
[6] T. Fujimoto, M.M. Matsushita, K. Awaga, J. Phys. Chem. C 116 (2012) 5240–5245.
[7] T. Fujimoto, M.M. Matsushita, K. Awaga, Appl. Phys. Lett. 97 (2010) 123303(1)–123303(3).
[8] A. Dadvand, F. Cicoira, K.Yu. Chernichenko, E.S. Balenkova, R.M. Osuna, F. Rosei, V.G. Nenajdenko, D.F. Perepichka, Chem. Commun. (2008) 5354–5356.
[9] J.H. Dopper, H. Wynberg, J. Org. Chem. 40 (1975) 1957–1966.
[10] G.V. Baryshnikov, N.N. Karaush, B.F. Minaev, Chem. Heterocycl. Compd. 50 (2014) 349–363.
[11] C.-N. Feng, M.-Y. Kuo, Y.-T. Wu, Angew. Chem. Int. Ed. 52 (2013) 7791–7794.
[12] Y. Sakamoto, T. Suzuki, J. Am. Chem. Soc. 135 (2013) 14074–14077.
[13] K.Yu. Chernichenko, V.V. Sumerin, R.V. Shpanchenko, E.S. Balenkova, V.G. Nenajdenko, Angew. Chem. Int. Ed. 45 (2006) 7367–7370.
[14] H. Erdtman, H.-E. Hogberg, Chem. Commun. (1968) 773–774.
[15] H. Erdtman, H.-E. Högberg, Tetrahedron Lett. (1970) 3389–3392.
[16] C.B. Nielsen, T. Brock-Nannestad, P. Hammershøj, T.K. Reenberg, M. Schau-Magnussen, D. Trpcevski, T. Hensel, R. Salcedo, G.V. Baryshnikov, B.F. Minaev, M. Pittelkow, Chem. Eur. J. 19 (2013) 3898–3904.
[17] T. Hensel, D. Trpcevski, C. Lind, R. Grosjean, P. Hammershoj, C.B. Nielsen, T. Brock-Nannestad, B.E. Nielsen, M. Schau-Magnussen, B. Minaev, G.V. Baryshnikov, M. Pittelkow, Chem. Eur. J. 19 (2013) 17097–17102.
[18] A. Rajca, M. Miyasaka, S. Xiao, P.J. Boratynski, M. Pink, S. Rajca, J. Org. Chem. 74 (2009) 9105–9111.
[19] T. Ohmae, T. Nishinaga, M. Wu, M. Iyoda, J. Am. Chem. Soc. 132 (2010) 1066–1074.
[20] T. Torroba, M. García-Valverde, Angew. Chem. Int. Ed. Engl. 45 (2006) 8092–8096.
[21] K. Aita, T. Ohmae, M. Takase, K. Nomura, H. Kimura, T. Nishinaga, Org. Lett. 15 (2013) 3522–3525.
[22] C.F. Wilcox Jr., J.P. Uetrecht, K.G. Grohmann, J. Am. Chem. Soc. 94 (1972) 2532–2533.
[23] I. Willner, M. Rabinovitz, Org. Chem. 45 (1980) 1628–1633.
[24] X.-D. Xiong, C.-L. Deng, X.-S. Peng, Q. Miao, H.N.C. Wong, Org. Lett. 16 (2014) 3252–3255.
[25] B.F. Minaev, G.V. Baryshnikov, V.A. Minaeva, Comput. Theor. Chem. 972 (2011) 68–74.
[26] G.V. Baryshnikov, B.F. Minaev, V.A. Minaeva, A.T. Baryshnikova, J. Mol. Struct. 1026 (2012) 127–132.
[27] G.V. Baryshnikov, B.F. Minaev, M. Pittelkow, C.B. Nielsen, R. Salcedo, J. Mol. Model. 19 (2013) 847–850.
[28] G.V. Baryshnikov, B.F. Minaev, V.A. Minaeva, V.G. Nenajdenko, J. Mol. Model. 19 (2013) 4511–4519.
[29] G.V. Baryshnikov, R.R. Valiev, N.N. Karaush, B.F. Minaev, Phys. Chem. Chem. Phys. 16 (2014) 15367–15374.
[30] V.A. Minaeva, B.F. Minaev, G.V. Baryshnikov, O.M. Romeyko, M. Pittelkow, Vib. Spectrosc. 65 (2013) 147–158.
[31] V.A. Minaeva, B.F. Minaev, G.V. Baryshnikov, H. Agren, M. Pittelkow, Vib. Spectrosc. 61 (2012) 156–166.
[32] V.A. Minaeva, B.F. Minaev, G.V. Baryshnikov, O.N. Romeyko, M. Pittelkow, J. Appl. Spectrosc. 79 (2012) 695–707.
[33] N.N. Karaush, B.F. Minaev, G.V. Baryshnikov, V.A. Minaeva, Opt. Spectrosc. 116 (2014) 33–46.
[34] V.A. Minaeva, B.F. Minaev, G.V. Baryshnikov, M. Pittelkow, Opt. Spectrosc. 114 (2013) 509–521.
[35] L.-W. Shi, B. Chen, J.-H. Zhou, T. Zhang, Q. Kang, M.-B. Chen, J. Phys. Chem. A 112 (2008) 11724–11730.
[36] T.N. Gribanova, N.S. Zefirov, V.I. Minkin, Pure Appl. Chem. 82 (2010) 1011–1024.
[37] T.K. Mandal, D. Jose, A. Nijamudheen, A. Datta, J. Phys. Chem. C 118 (2014) 12115–12120.
[38] B. Napolion, F. Hagelberg, M.-J. Huang, J.D. Watts, T.M. Simeon, D. Vereen, W.L. Walters, Q.L. Williams, J. Phys. Chem. A 115 (2011) 8682–8690.
[39] G. Baryshnikov, B. Minaev, N. Karaush, V. Minaeva, RSC Adv. 4 (2014) 25843–25851.
[40] G. Baryshnikov, B. Minaev, N. Karaush, V. Minaeva, Phys. Chem. Chem. Phys. 16 (2014) 6555–6559.

[41] R. Salcedo, L.E. Sansores, A. Pïcazo, L. Sansón, J.U. Mol, Struct. Theochem. 678 (2004) 211–215.
[42] T.N. Gribanova, N.S. Zefirov, V.I. Minkin, Doklady Chem. 426 (2009) 105–110.
[43] X. Xiong, C.-L. Deng, B.F. Minaev, G.V. Baryshnikov, X.-S. Peng, H.N.C. Wong, Chem. Asian J. 9 (2014), http://dx.doi.org/10.1002/asia.201403028.
[44] A.D. Becke, J. Chem. Phys. 98 (1993) 5648–5652.
[45] C. Lee, W. Yang, R.G. Parr, Phys. Rev. B 37 (1988) 785–789.
[46] K. Raghavachari, J.S. Binkley, R. Seeger, J.A. Pople, J. Chem. Phys. 72 (1980) 650–654.
[47] M.J. Frisch, G.W. Trucks, H.B. Schlegel, G.E. Scuseria, M.A. Robb, J.R. Cheeseman, G. Scalmani, V. Barone, B. Mennucci, G.A. Petersson, H. Nakatsuji, M. Caricato, X. Li, H.P. Hratchian, A.F. Izmaylov, J. Bloino, G. Zheng, J.L. Sonnenberg, M. Hada, M. Ehara, K. Toyota, R. Fukuda, J. Hasegawa, M. Ishida, T. Nakajima, Y. Honda, O. Kitao, H. Nakai, T. Vreven, J.A. Montgomery, Jr., J.E. Peralta, F. Ogliaro, M. Bearpark, J.J. Heyd, E. Brothers, K.N. Kudin, V.N. Staroverov, R. Kobayashi, J. Normand, K. Raghavachari, A. Rendell, J.C. Burant, S.S. Iyengar, J. Tomasi, M. Cossi, N. Rega, J.M. Millam, M. Klene, J.E. Knox, J.B. Cross, V. Bakken, C. Adamo, J. Jaramillo, R. Gomperts, R.E. Stratmann, O. Yazyev, A.J. Austin, R. Cammi, C. Pomelli, J.W. Ochterski, R.L. Martin, K. Morokuma, V.G. Zakrzewski, G.A. Voth, P. Salvador, J.J. Dannenberg, S. Dapprich, A.D. Daniels, O. Farkas, J.B. Foresman, J.V. Ortiz, J. Cioslowski, D.J. Fox, Gaussian Inc, Wallingford CT, Gaussian 09. Rev. A.02 (2009).
[48] P.L. Polavarapu, J. Phys. Chem. 94 (1990) 8106–8112.
[49] E. Runge, E.K.U. Gross, Phys. Rev. Lett. 52 (1984) 997–1000.
[50] S. Miertuš, E. Scrocco, J. Tomasi, Chem. Phys. 55 (1981) 117–129.
[51] S.I. Gorelsky, SWizard program, <http://www.sg-chem.net>, University of Ottawa, Ottawa, Canada, 2013.
[52] Z. Chen, C.S. Wannere, C. Corminboeuf, R. Puchta, P.v.R. Schleyer, Chem. Rev. 105 (2005) 3842–3888.
[53] B. Bak, D. Christensen, L. Hansen-Nygaard, J. Rastrup-Andersen, J. Mol. Spectrosc. 7 (1961) 58–63.
[54] N.M. Pozdeev, O.B. Akulinin, A.A. Shapkin, N.N. Magdesieva, J. Struct. Chem. 11 (1970) 804–809.
[55] S. Gundersen, S. Samdal, T.G. Strand, H.V. Volden, J. Mol. Struct. 832 (2007) 164–171.
[56] D.S. Kummli, S. Lobsiger, H.M. Frey, S. Leutwyler, J.F. Stanton, J. Phys. Chem. A 112 (2008) 9134–9143.
[57] G. Socrates, Infrared and Raman Characteristic Group Frequencies: Tables and Charts, John Wiley & Sons Ltd., 2001.
[58] L. Goodman, A.G. Ozkabak, S.N. Thakur, J. Phys. Chem. 95 (1991) 9044–9058.
[59] The official web site of National Institute of Advanced Industrial Science and Technology (AIST), Research Information Database (RIO-DB). <http://riodb.ibase.aist.go.jp/riohomee.html>.
[60] J.S. Kwiatkowski, J. Leszczynski, I. Teca, J. Mol. Struct. 436–437 (1997) 451–480.
[61] S. Radenković, I. Gutman, P. Bultinck, J. Phys. Chem. A 116 (2012) 9421–9430.
[62] J. Yu, Q. Sun, Y. Kawazoe, P. Jena, Nanoscale (2014), http://dx.doi.org/10.1039/C4NR05037A.
[63] E. Kleinpeter, A. Koch, S. Schulz, P. Wacker, Tetrahedron 70 (2014) 9230–9239.
[64] H. Fliegl, S. Taubert, O. Lehtonen, D. Sundholm, Phys. Chem. Chem. Phys. 13 (2011) 20500–20518.
[65] Y.L. Li, K.H. Leung, D.L.J. Phillips, J. Phys. Chem. A 105 (2001) 10621–10625.
[66] P.Z. Zhu, S.Y. Ong, P.Y. Chan, K.H. Leung, D.L.J. Phillips, J. Am. Chem. Soc. 123 (2001) 2645–2649.